2016

The Dynamics of Electron-Induced Formation of N-2 and N-3 Species from Condensed Ammonia

Jane Zhu
jzhu3@wellesley.edu

The Dynamics of Electron-Induced Formation of N-2 and N-3 Species from Condensed Ammonia

Jane L. Zhu

Advisor: Christopher R. Arumainayagam, Ph.D.

Department of Chemistry, Wellesley College

Submitted in Partial Fulfillment of the

Prerequisites for Honors in Chemistry

April 2016

Acknowledgements

First and foremost, I have nothing but the utmost thanks for my advisor, Chris Arumainayagam. You have taught me so much over the past four years. Thank you for always pushing me to be a better scholar and scientist. More importantly, thank you for believing in me.

Thank you to my thesis committee – Professor Mala Radhakrishnan and Professor Carla Verschoor. Your constructive criticisms, advice, and encouragement have been tremendously helpful during this process, especially during some of the more frustrating and stressful times. Thank you also to Professor Ellen Hildreth for graciously agreeing to serve as my honors visitor.

Many thanks to the incredible chemistry department and science center staff. Thank you Professor Paul Reisberg for your immense support over the last several years. Special thanks to George Dai, Larry Knowles, and John DeBolt – you all have been so gracious with your time and efforts, especially when problems arose with our ultrahigh vacuum chamber.

I would also like to thank my brilliant lab mates. Without you all, this thesis would not have been possible. Thank you all for always being so willing to come into lab bright and early in the morning and staying until midnight to help me with experiments and data analysis. I will miss you all dearly. I also cannot overstate my gratitude for my former lab mates, Katie Shulenberger'14 and Katherine Tran'15, for starting this ammonia project. Thank you for your invaluable guidance.

A heartfelt thanks to my wonderful friends for putting up with me. To my chemistry major friends, especially Hannah Sim, Hikari Murayama, Darlene Dang, and Amy Yuan – you all have made my classes the past four years so much fun. I will miss studying with you all and having someone to go to Starbucks with every day. Thank you to Caroline Chang, Lois Kwon, Rachel Han, Rebecca Chen, and Wanyi Li for dragging me out of the science center and keeping me sane this past year.

I am so grateful for our friendships. Thank you also to Frieda Zhang'15 for being my big sister away from home. You always give the greatest advice and Wellesley has not been the same since you have graduated.

Last but not least, I would like to extend thanks to my family. Mom and Dad – I am forever in debt to you both for all of the sacrifices the two of you have made over the years to help make my dreams and goals a reality. Lin – thank you for being such a wonderful role model. I don't think I could have survived Wellesley without your guidance and support. Elizabeth – thank you for your love and support. More importantly, thank you for being my best friend. I hope I make y'all proud.

Table of Contents

Table of Figures

Abstract

We have previously shown that low-energy (50 eV) electron-induced oligomerization of condensed carbon tetrachloride (CCl_4) can produce species with six or more carbons [1]. In the study described herein, using post-irradiation temperature-programmed desorption (TPD) experiments, we examine the electron-induced oligomerization of condensed ammonia to yield hydrazine (N_2H_4), diazene (N_2H_2), cyclotriazane/triazene (N_3H_3), and triazane (N_3H_5). To understand the dynamics of oligomerization, we have investigated the dependence of these reaction products' yields on irradiation time, film thickness, electron energy, and incident electron flux. Our yield versus irradiation/film thickness results are consistent with the previously proposed bimolecular mechanisms of formation for hydrazine and diazene. In contrast, yield versus irradiation time results for triazane suggest that it is a tertiary radiolysis product. Furthermore, although triazane was produced in relatively large quantities at an incident electron energy of 1000 eV, none was produced at 500 eV for all explored variations of experimental parameters (film thickness, irradiation time, and electron flux). We attribute this high apparent threshold incident electron energy to the dose rate effect, which violates the Bunsen-Roscoe Law, according to which a photochemical effect is directly proportional to the total energy dose, irrespective of the time required to deliver that dose. We have investigated the dose rate effect observed in ammonia radiolysis by varying the irradiation flux while maintaining a constant fluence. These results provide a basis from which we can begin to understand not only the dose rate effect in electron-induced reactions but also the mechanisms by which more complex nitrogen-containing species are formed.

1 Introduction

1.1 Astrochemical relevance and motivation for investigating ammonia

The interstellar medium (ISM) is known for its dark, cold, and sparse regions. In fact, temperatures in the interstellar medium can reach as low as 10 K [2-5]. Thus, the interstellar medium is often considered to be an unlikely site for chemical reactions. However, contrary to popular thought, the interstellar medium is a dynamic arena where intricate chemistry takes place. In the cosmic chemistry cycle, diffuse molecular clouds condense into dense molecular clouds to ultimately form stars and planets. The remnants of dying stars allow for the formation of new clouds and the continuation of the cycle. Dark, dense molecular clouds are thought to be the chemical factory of the interstellar medium, where prebiotic molecules such as aminoacetonitrile, glycoaldehyde, and glycolylurea are synthesized [6-11].

Ammonia (NH_3) is of particular astrochemical interest due to its presence in a wide range of locations in outer space. Significant amounts of ammonia have been detected in the atmospheres of Jupiter [12], Saturn [12], Uranus [13], and Neptune [14] as well as on the surface of Saturn's moon, Enceladus [15]. Additionally, cometary ices in the Halley, Borrelly, Hartley-Good, and Thiele comets have been found to contain a substantial amount of ammonia (>10%) [16]. Studies of interstellar ice compositions in protostellar regions have revealed that the abundance of ammonia relative to water is 1–10%, making ammonia the most dominant nitrogen-containing compound in interstellar ices [17]. Although the amount of ammonia in these ices is lower than that of carbon monoxide and carbon dioxide, it is considerably greater than that of methane and methyl formate [18, 19]. The relatively high abundance of ammonia in star-forming regions suggests that ammonia may serve as a precursor to biologically relevant, nitrogen-containing

molecules such as cyanomethanimine (NC_2HNH), which has been detected in the interstellar gas cloud, Sgr B2(N) [20]. Thus, by studying the radiolysis of ammonia, we aim to better understand the mechanisms by which more complex prebiotic molecules can be formed in the interstellar medium.

1.2 Electron-induced cosmic ice chemistry

In the interstellar medium, 100 monolayers-thick cosmic ices containing water (H_2O), carbon dioxide (CO_2), methanol (CH_3OH), and ammonia (NH_3) surround carbonaceous or silicaceous micron-size dust particles [21]. These ices are continuously bombarded by cosmic rays and other forms of high-energy radiation. Previous astrochemical studies have focused primarily on the photon-induced chemistry of cosmic ices**,** and many species detected in the interstellar medium have been attributed solely to photon chemistry. However, in our laboratory, we hypothesize that low-energy electrons may also play a role in the synthesis of molecules found in space.

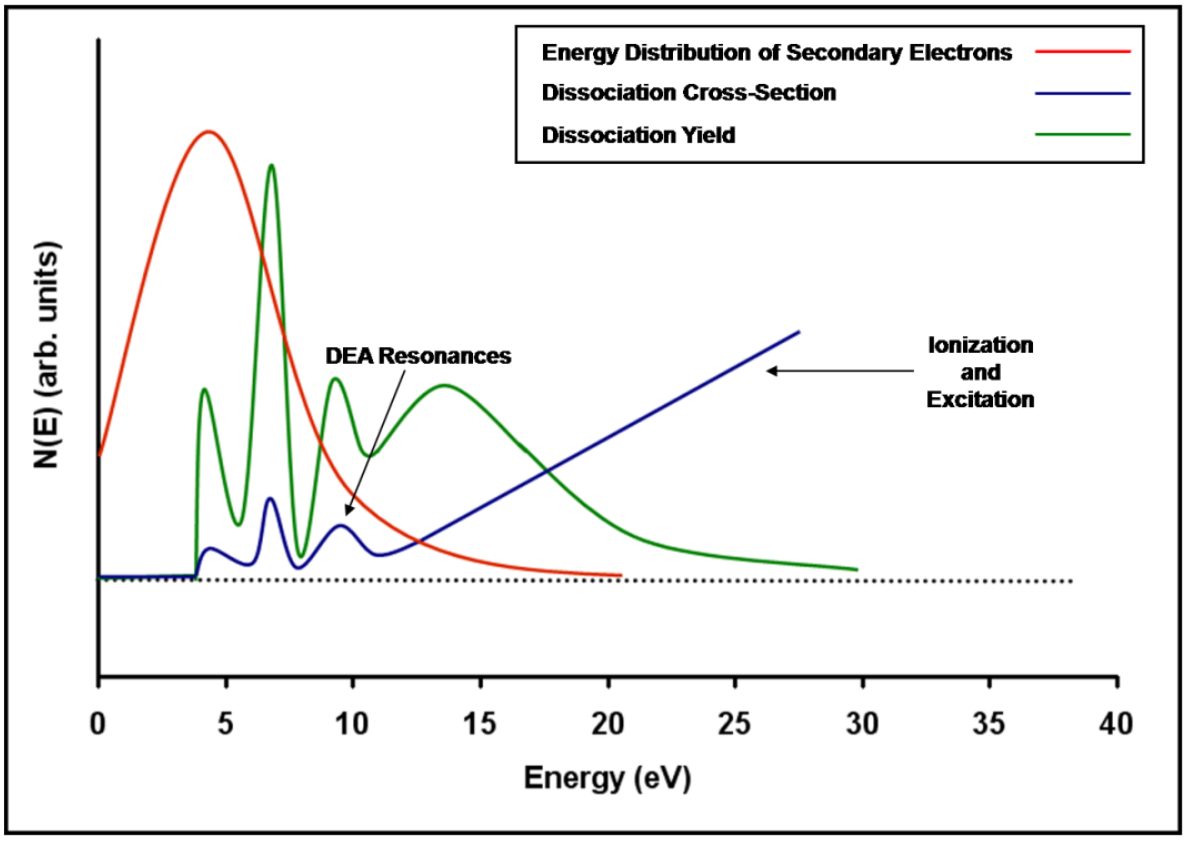

Figure 1

Importance of low-energy electrons. Energy distribution of secondary electrons (red); dissociation cross-section (blue); dissociation yield (green) was obtained by multiplying the energy distribution by the dissociation cross-section. Reproduced from [22].

When high-energy (E_{max} ~ 10^{20} eV) radiation is incident on matter such as cosmic ices, a cascade of secondary electrons is produced. The energy distribution of these secondary electrons reveals that the majority of these electrons have energies below 15 eV [22]. The dissociation cross-section, which is the likelihood that the molecule will dissociate upon impact of an electron, can be multiplied by this energy distribution to obtain the dissociation yield. As indicated in Figure 1, the dissociation yield overwhelmingly favors the low-energy range below 15 eV. As a result, it is thought that these low-energy electrons are the driving force behind the high-energy radiation-induced dissociation and synthesis of molecules [22]. Moreover, electron-induced reactions may

produce species that are not necessarily accessible via photon-induced chemistry, as described in detail later on.

When an electron is incident on a generic molecule AB, it may dissociate the molecule in one of three reaction pathways:

The first mechanism is *electron impact excitation*, which occurs at energies above ~ 3 eV. In this reaction channel, an incident electron transfers energy to the AB molecule and yields a molecule in an excited state (AB*) (Equation 1).

$$e^- + AB \rightarrow AB^* + e^- \qquad (1)$$

AB* can subsequently release energy to return to its original ground state or undergo dissociation. One possible dissociation pathway is dipolar dissociation, where the excited molecule dissociates into an anion and a cation.

Another reaction mechanism the AB molecule can undergo upon impact of an electron is *electron impact ionization*, which occurs at incident electron energies above approximately 10 eV (Equation 2).

$$e^- + AB \rightarrow AB^{+*} + 2e^- \qquad (2)$$

When the electron bombards the molecule, it ejects an additional electron, forming an excited cation, which can then dissociate into a radical and a cation.

In the last reaction pathway, *electron attachment*, a temporary negative ion (TNI) is formed (Equation 3). This reaction channel is perhaps the most important, as it is exclusive to electron-induced reactions. Electron attachment typically occurs at energies below 15 eV.

$$e^- + AB \rightarrow AB^- \qquad (3)$$

Depending on the lifespan of the temporary negative ion, it can undergo autodetachment, dissociative attachment, or associative attachment.

The three dissociation mechanisms described above are summarized in Figure 2 below.

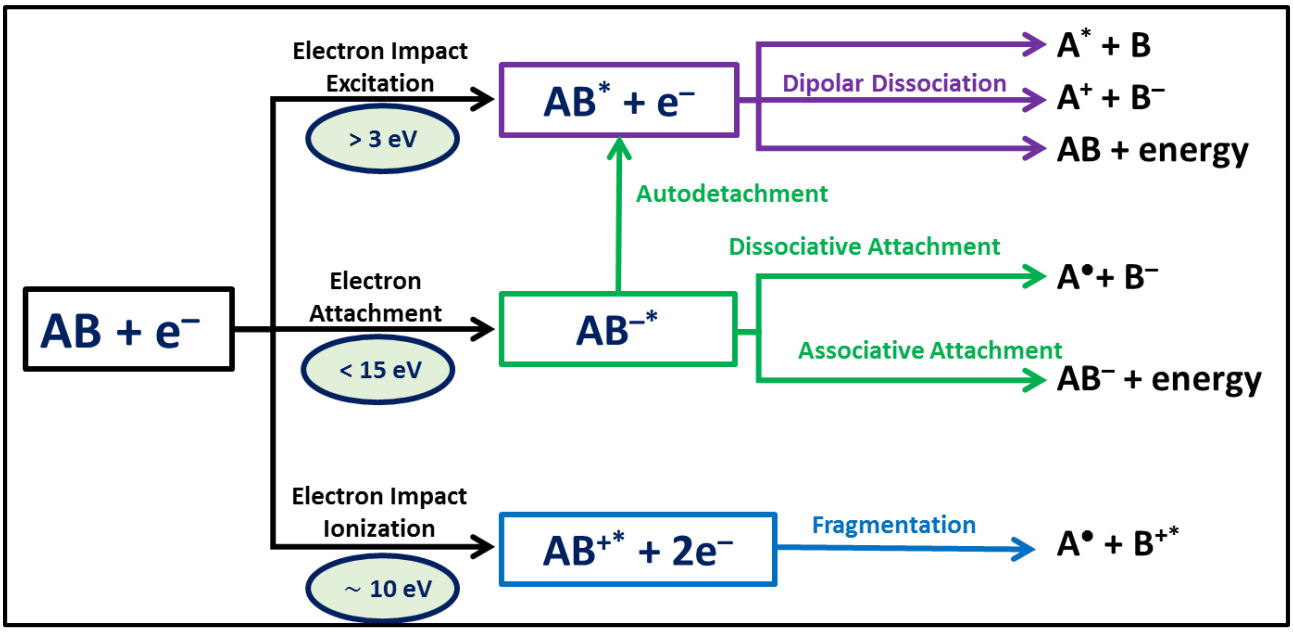

Figure 2

Dissociation mechanisms of a generic molecule AB when bombarded with an electron. Adapted from [23].

Another key difference between photon-induced chemistry and electron-induced chemistry is the allowed electronic transitions. When a molecule is excited via photons, the electric dipole selection rule nominally forbids singlet to triplet transitions. However, because electrons are indistinguishable, this selection rule does not apply to species that are excited by electrons. Thus, the spin of the HOMO electron need not be conserved as it transitions into the LUMO. Consequently, there may be electron-induced reaction products that are not accessible via photon-induced reactions. For example, the electron-induced production of methoxymethanol

(CH_3OCH_2OH) from condensed methanol has been observed [24]. In contrast, UV photon studies have failed to identify methoxymethanol as a photolysis product of condensed methanol [25-29].

1.3 Previous Studies of the Electron-Induced Formation of N-2 Species from Condensed Ammonia

Previous studies of the electron-induced reactions of condensed ammonia have reported the production of hydrazine (N_2H_4) and diazene (N_2H_2) following irradiation with high-energy (5000 eV) incident electrons [30]. The following mechanisms for the formation of these two species have been proposed.

Hydrazine is thought to form from the combination of two NH_2 radicals (Figure 3) [30].

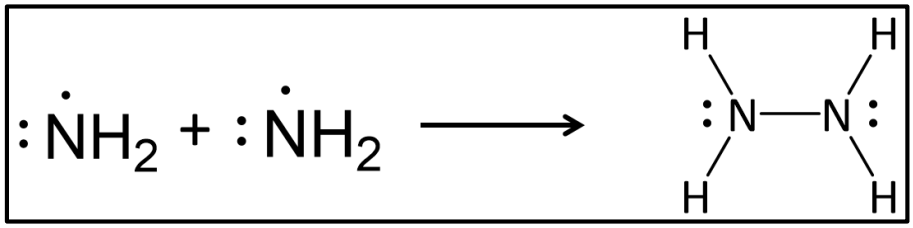

Figure 3
Proposed mechanism for hydrazine formation involves two NH_2 radicals joining together [30].

Similarly, it has been proposed that two NH radicals combine together to yield diazene (Figure 4A). However, it has also been hypothesized that an excited hydrazine molecule can dissociate to yield H_2 and diazene (Figure 4B) [30].

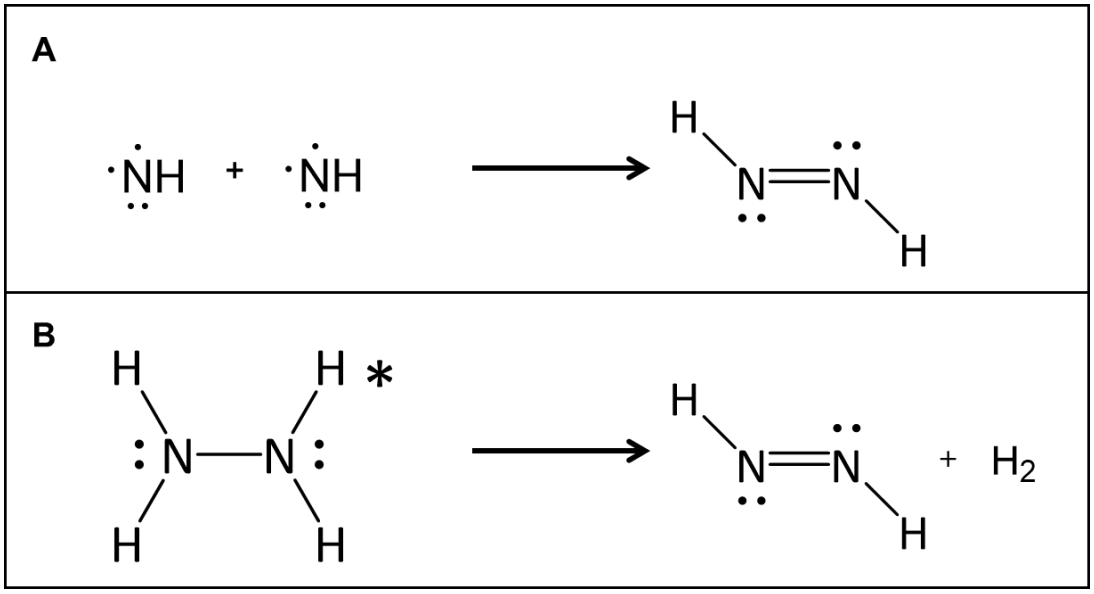

Figure 4

Proposed mechanisms for diazene formation. The first involves two NH radicals joining together (a). The second suggests that diazene is formed from the dissociation of an excited hydrazine molecule (b) [30].

Experiments conducted in our laboratory have found more convincing evidence for the electron-induced production of hydrazine and diazene from condensed ammonia [31].

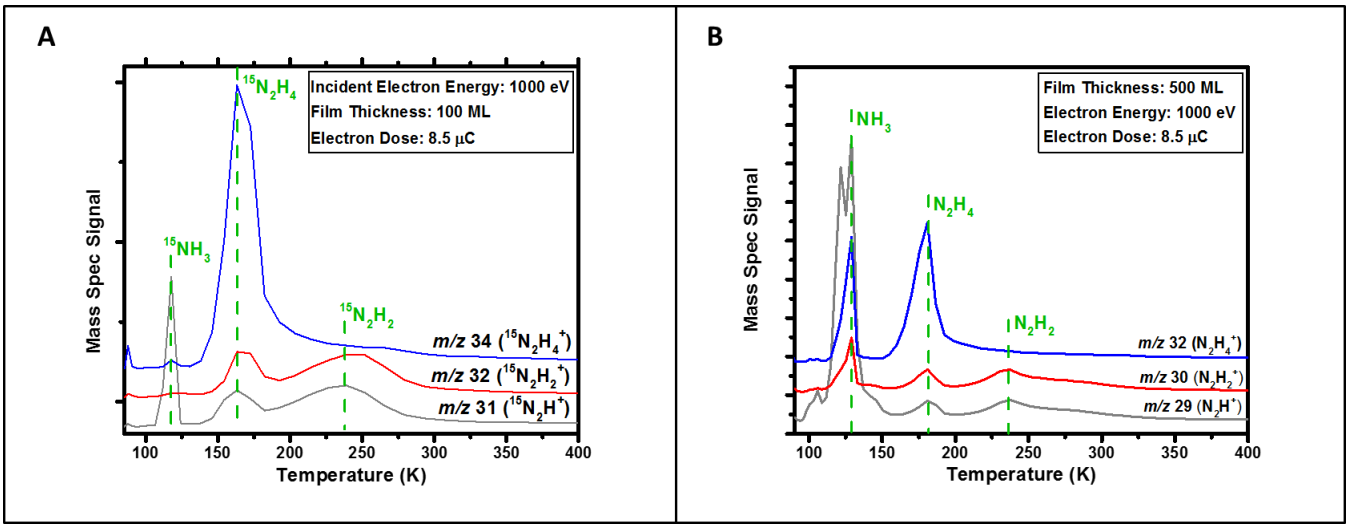

Figure 5

Post-irradiation temperature programmed desorption results following electron irradiation of $^{15}NH_3$ (a) and NH_3 (b) films with 1000 eV electrons [31]. The peak at approximately 125 K is due to the desorbing ammonia undergoing ion-molecule reactions in the mass spectrometer.

These identifications of hydrazine and diazene were confirmed by using isotopologues ($^{15}NH_3$, ND_3, and NH_3) of ammonia in our previous studies (Figure 5) [31].

1.4 Previous Studies of the Electron-Induced Formation of N-3 Species from Condensed Ammonia

Potential N-3 radiolysis products of ammonia include hydrazoic acid (N_3H), cyclotriazane (N_3H_3), triazene (N_3H_3), triimide ($N_3H_3^{2-}$), and triazane (N_3H_5) (Figure 6).

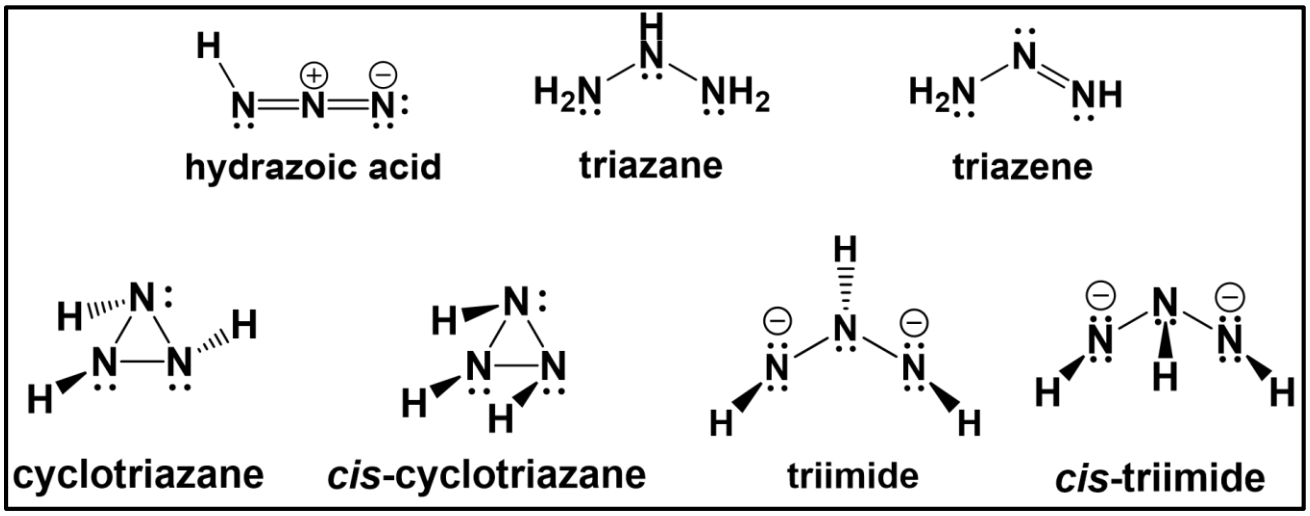

Figure 6
Potential N-3 radiolysis products of condensed ammonia

Our earlier search for the electron-induced formation of hydrazoic acid, the most stable of the N-3 species, yielded null results [31]. A search for the other highly unstable N-3 species was not conducted previously in our laboratory.

In 2015, experimental evidence was published for the production of triazane (N_3H_5) following 5000 eV electron-irradiation of condensed ammonia [32]. Reflectron time-of-flight mass spectrometry, a state of the art technique, was used to conduct these post-irradiation temperature programmed desorption experiments. The technique is based on the fact that heavier ions take a longer time to reach the detector than do lighter ions. As a result, a time-of-flight mass

spectrometer determines the mass-to-charge ratio of an ion by recording the time it takes for an ion to travel through the flight path. A time-of-flight mass spectrometer has several advantages over a traditional quadrupole mass spectrometer, which is often limited by its spectral acquisition rate. This issue is further exacerbated at higher masses. In contrast to quadrupole mass spectrometry, time-of-flight mass spectrometry does not require a voltage scan in order to select for ions with particular mass-to-charge ratios. In fact, in time-of-flight mass spectrometry, almost all of the ions reach the detector in a significantly shorter period of time [33]. The addition of a mass-reflectron further enhances the resolving power of the instrument by increasing the flight path length, effectively increasing the flight time for ions [34]. This increase in flight time results in a larger temporal distribution between ions with similar mass-to-charge ratios.

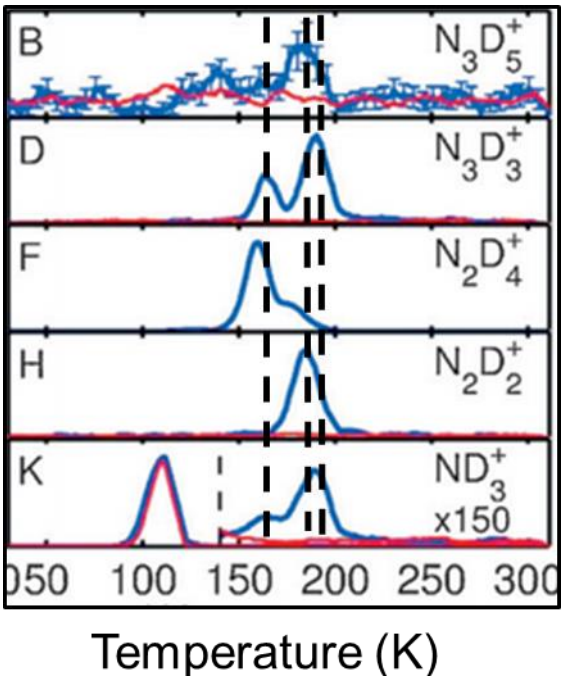

Figure 7

Post-irradiation temperature programmed desorption data following the irradiation of a 500 nm film of ND_3 with 5000 eV electrons. Modified from [32]. Black dashed lines were added to original post-irradiation temperature programed desorption data. Only ND_3 data from the original publication is shown.

In the recently published post-irradiation temperature programmed desorption data (Figure 7), the *m*/*e* = 52 peak was attributed to deuterated triazane (N_3D_5) [32]. Furthermore, the temperature programmed desorption curve for *m/e* = 48 ($N_3D_3^+$) revealed two peaks. The higher temperature *m/e* = 48 peak was thought to be a fragment of triazane while two possibilities for the lower temperature *m/e* = 48 peak were proposed: cyclotriazane and triazene.

Additionally, theoretical *ab initio* electronic structure calculations using the hybrid density functional B3LYP level of theory with the cc-pVTZ basis set were performed to study the potential energy surface of triazane [35]. Investigations on the decomposition reaction pathways of triazane revealed that triazane is a labile product; it is thermodynamically unstable, but kinetically stable [32]. Thus, while triazane is a relatively unstable molecule, the energy barrier it needs to overcome in order to decompose to smaller species (*i.e.* hydrazine, diazene, and nitrene) allows for its detection in post-irradiation temperature programmed desorption experiments [32].

Previous theoretical studies have also investigated these N-3 species in order to better understand their thermodynamic and kinetic stabilities [36]. Various isomers of N_3H_3 including triazene, triimide, *cis*-triimide, cyclotriazane, and *cis*-cyclotriazane have been studied in order to determine whether there are indeed stable isomers of N_3H_3 that can potentially exist in the gas phase (Figure 6). *Ab initio* calculations using the DZP-SCF basis set have allowed for the computation and comparison of the enthalpies of formation ($\Delta H_f°$) for each of the previously listed N_3H_3 species [36].

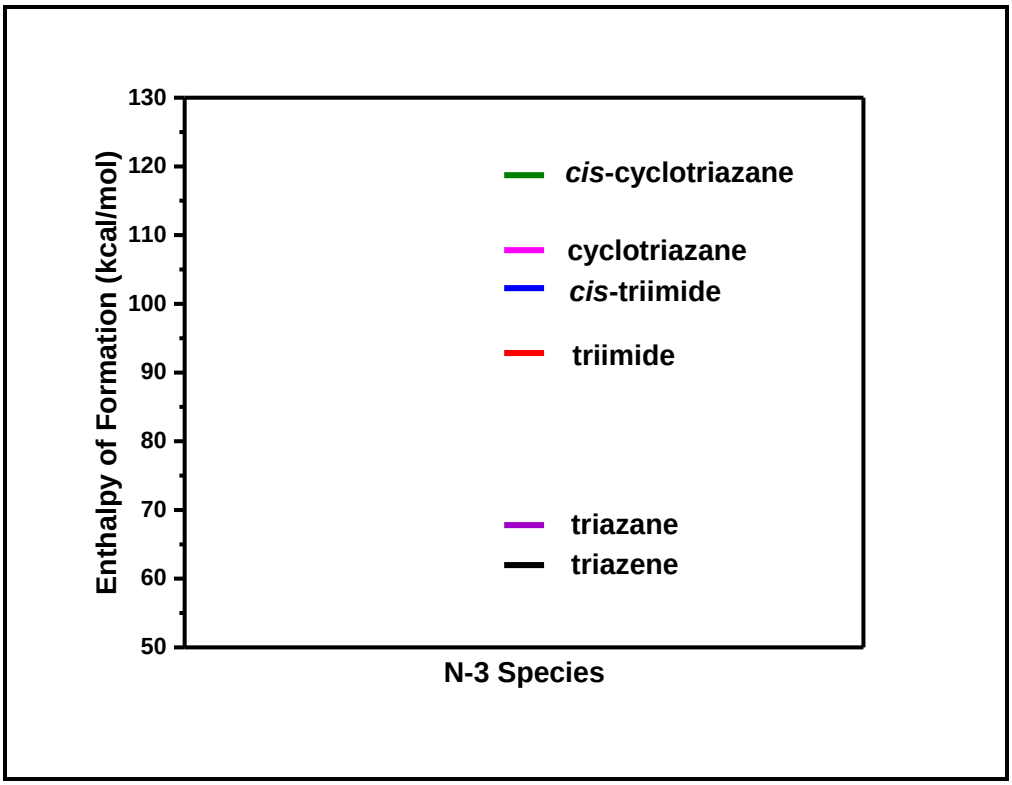

Figure 8

The enthalpies of formation (kcal/mol) calculated for possible N-3 radiolysis products [35, 36].

The enthalpy of formation for triazene, the most stable of the N_3H_3 isomers, was determined to be 61.97 kcal/mol. In comparison, the enthalpies of formation for triimide, *cis*-triimide, cyclotriazane, and *cis*-cyclotriazane were calculated to be 92.84 kcal/mol, 102.28 kcal/mol, 107.81 kcal/mol, and 118.72 kcal/mol, respectively. As such, it can be anticipated that the N_3H_3 isomers in decreasing order of stability are as follows: triazene, triimide, *cis*-triimide, cyclotriazane, and *cis*-cyclotriazane. Analogous *ab initio* calculations using the Møller-Plesset pertubation theory with the 6-31G* basis set determined the enthalpy of formation for triazane to be 67.8 kcal/mol [35]. Although thermodynamic stability is typically based on both enthalpy and entropy, a comparison of enthalpies to determine stability is sufficient due to the low temperature conditions in cosmic ices. Thus, the positive enthalpy of formation values for these N-3 species are consistent with their thermodynamic instabilities.

1.5 Bunsen-Roscoe Law of Reciprocity & Dose Rate Effect

As described in detail later, the results presented in this thesis suggest a violation of the Bunsen-Roscoe Law of Reciprocity, according to which a photochemical effect is directly proportional to the total energy dose, irrespective of the time required to deliver that dose. However, it has been observed that radiation chemistry does not always obey this law. Perhaps the most well-known example of a dose rate effect is the administration of radiation therapies for cancer patients. When a radiation dose is delivered for patients in a short amount of time, many patients suffer side effects from the radiation as their DNA is not given sufficient time to repair any damage the radiation has caused. However, when the same dose is delivered over a longer period of time, patients often experience less severe cases of radiation sickness [37].

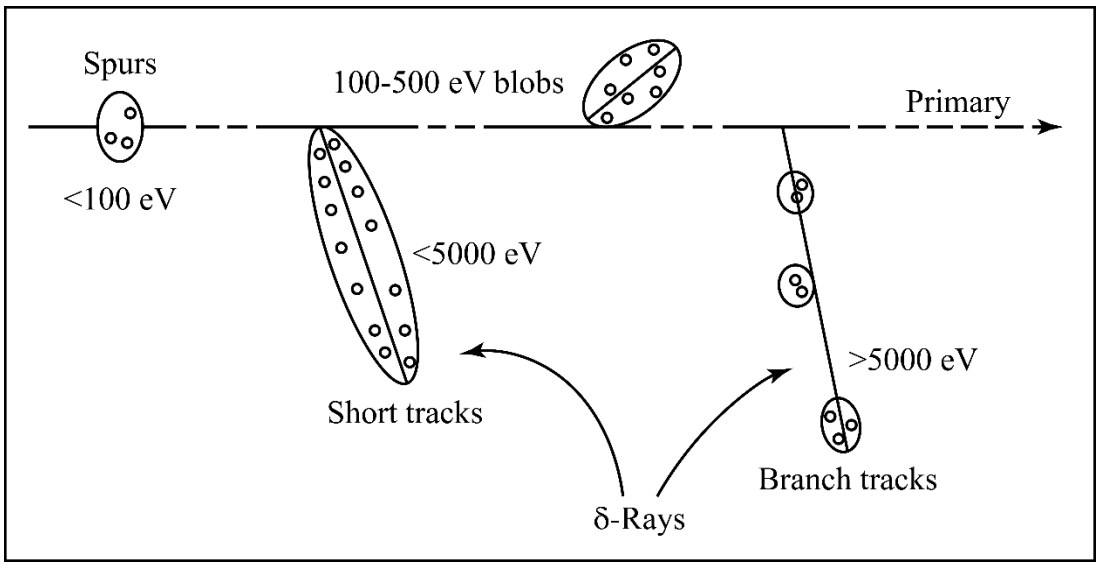

Figure 9

A low linear energy transfer track is shown. This track consists of four types of entities – spurs, blobs, short tracks, and branch strops. Short tracks and branch tracks are referred to as δ-rays. Adapted from [38].

Similarly, the radiolysis of ammonia by electrons may also be governed by a dose rate effect, which can be best explained via the linear energy transfer of an electron. The linear energy transfer

(LET) of radiation refers to the energy per unit track length deposited by an ionizing entity in a medium. Depending on the energy of the initial primary electrons, theoretical studies have predicted that radiation with low linear energy transfer such as electrons can produce three non-overlapping types of regions: spurs (< 100 eV), blobs (~ 100 eV to 500 eV), and short tracks (~ 500 eV to 5000 eV) (Figure 9) [38]. We hypothesize that radicals close in proximity to each other within the blobs are responsible for the dose rate effect observed during the electron irradiation of condensed ammonia.

2 Experimental

All experiments were conducted in a custom-designed stainless steel ultrahigh vacuum (UHV) chamber, as described in a previous thesis [39] (Figure 10). The base pressure of the UHV chamber is maintained at ~ 1×10^{-9} Torr, and is monitored with an ion gauge. In order to maintain ultrahigh vacuum pressures, a turbomolecular pump, rotary vane mechanical pump, ion pump, and titanium sublimation pump are employed. A Ta(110) crystal substrate inside the chamber is cooled via a liquid nitrogen reservoir to cryogenic temperatures of ~ 90 K. The crystal is fixed to a manipulator that is capable of θ, x, y, and z movement.

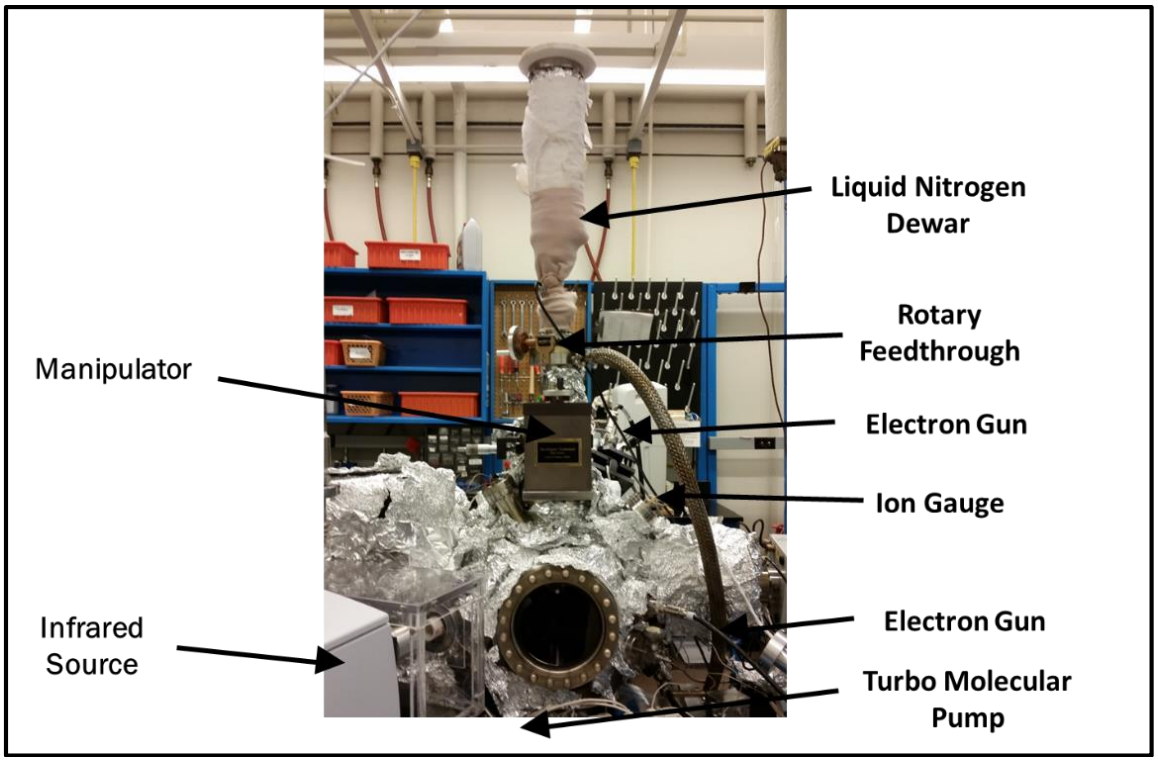

Figure 10

Ultrahigh vacuum (UHV) chamber used for post-irradiation temperature programmed desorption experiments.

Multilayer films of deuterated ammonia (ND_3, 99%, Cambridge Isotope Laboratories) are deposited upon the Ta(110) crystal substrate at approximately 90 K. This thin film growth is achieved by turning the cooled crystal to the dosing chamber from which gaseous deuterated ammonia is released into the ultrahigh vacuum chamber and allowed to condense onto the crystal. Ammonia film thicknesses range from 5 monolayers to 1000 monolayers and are determined by measuring the drop in pressure in the dosing chambers with a capacitance manometer (Granville-Phillips®, MSK instruments). One monolayer is defined to be 0.0009 Torr, as it is the maximum dosing chamber pressure drop that produced only a monolayer peak in temperature programmed desorption experiments. These films can then be subsequently irradiated with electrons ranging in energies from 2 eV to 1000 eV using a Kimball Physics FRA2X1-2 flood electron gun. The incident current used in our experiments range from 0.33 μA to 15 μA. The total electron dose, or

fluence, on a ND_3 film is defined to be the current incident on the crystal, or flux, multiplied by the irradiation time (Equation 4).

$$\text{Electron Dose } (\mu C) = \text{Incident Current } \left(\frac{\mu C}{s}\right) \times \text{Irradiation Time } (s) \quad (4)$$

The use of a Ta(110) crystal substrate requires slightly altered cleaning procedures from those used previously for our Mo(110) crystal substrate. Because both Mo(110) and Ta(110) are refractory metals, cleaning is relatively easy and simply requires heating to very high temperatures. To clean the crystal following each experiment, the Ta(110) crystal substrate is heated to 2200 K via radiative and electron bombardment heating. However, in contrast to Mo(110), a Ta(110) crystal substrate cannot be cleaned with oxygen to remove the buildup of carbon-based contaminants as oxygen can become embedded within the Ta(110) substrate itself [40].

Radiolysis products that desorb during irradiation can be monitored by electron-stimulated desorption experiments, which require turning the crystal to face the mass spectrometer and the electron gun simultaneously. Heavier products that remain in the film can be studied using post-irradiation analysis via two surface science techniques: temperature programmed desorption and infrared spectroscopy. Temperature programmed desorption experiments require heating the Ta(110) crystal substrate to sufficiently high temperatures to cause desorption of the radiolysis products. During heating, the remaining species that comprise the film can be detected using a Hiden IDP Series 500 quadrupole mass spectrometer**,** as each radiolysis product typically has a distinct desorption temperature.

3 Results and Discussion

3.1 Mo(110) and Ta(110) crystal substrates yield similar post-irradiation temperature programmed desorption results

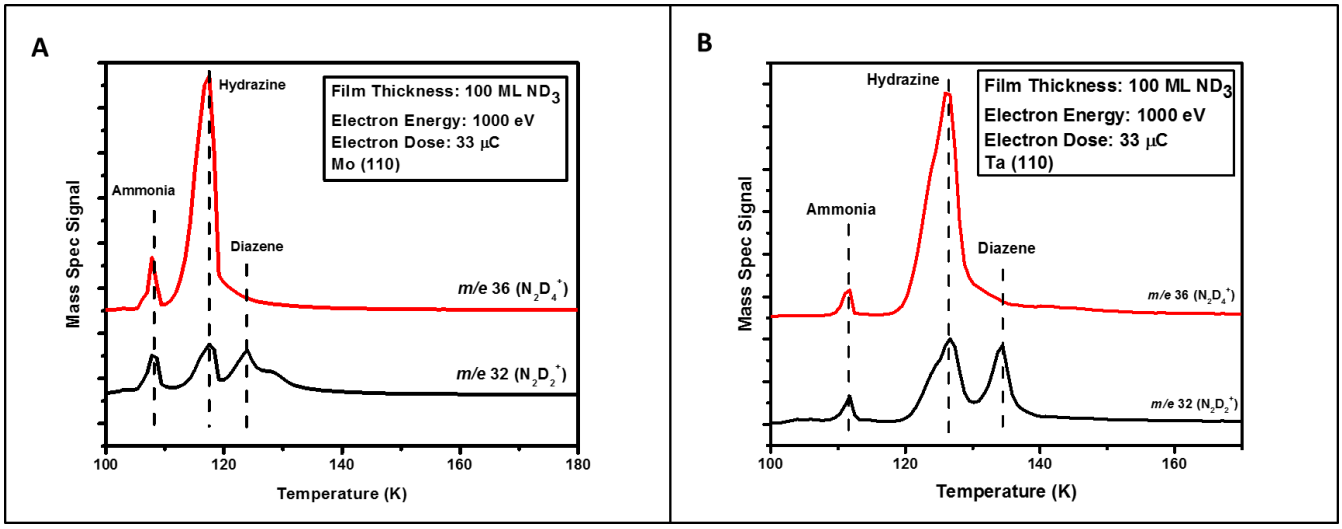

Figure 11

Post-irradiation temperature programmed desorption results of a 100 monolayer ND_3 film irradiated with 1000 eV electrons on a Mo(110) crystal substrate (a) and a Ta(110) crystal substrate (b).

To investigate the role of the metal substrate surface, ammonia radiolysis experiments were conducted with both Mo(110) and Ta(110) crystals. Both hydrazine and diazene were produced following electron radiolysis of an ammonia film regardless of the substrate (Figure 11). Furthermore, their desorption peaks appear qualitatively similar on both substrates, suggesting that the electron-induced reactions involved in producing these two species likely occur in the bulk of the thin film and not on the metal surface. We attribute the difference in desorption temperatures to different heating rates.

3.2 Identification of Triazane

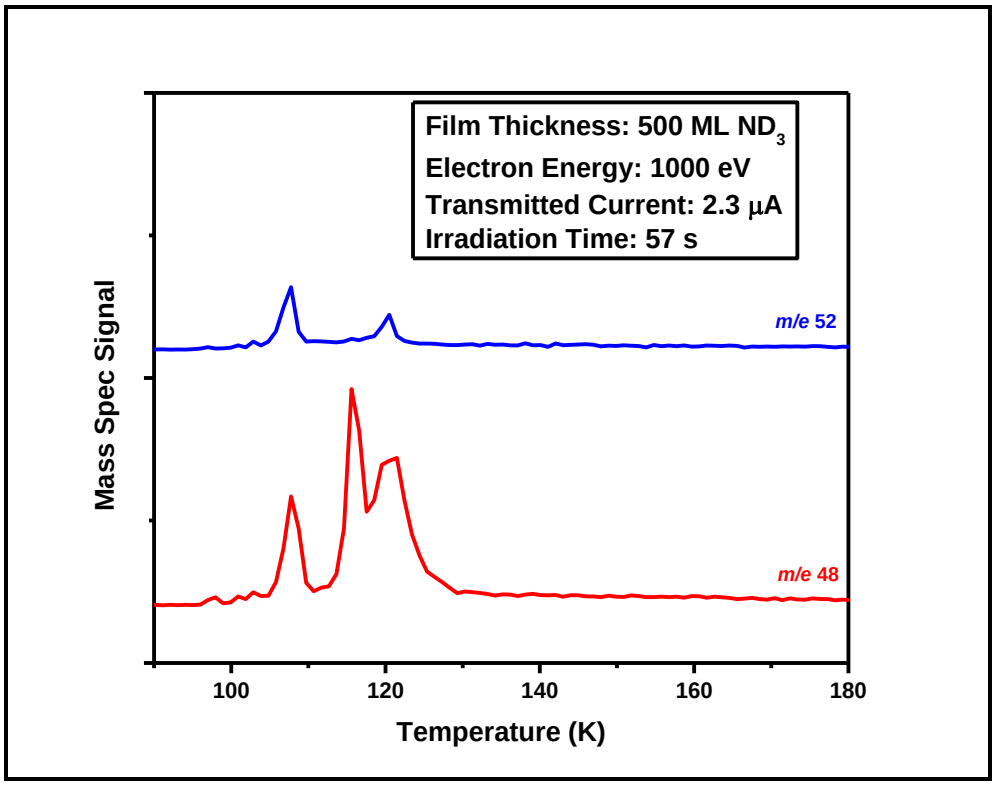

Figure 12

Post-irradiation temperature programmed desorption results of a 500 monolayer ND_3 film irradiated with 1000 eV electrons for 57 seconds at a dose rate of 2.3 μC/s. Difference in desorption temperatures compared to Figure 11 are due to a change in heating rate.

The electron-induced N-3 radiolysis products of condensed ammonia were identified using the results of post-irradiation temperature-programmed desorption experiments. The desorption peak at ~125 K in the *m/e* = 52 ($N_3D_5^+$) signal is assigned to triazane (N_3D_5), consistent with previous findings (Figure 12) [32]. Clearly, the desorption features observed for *m*/*e* = 48 ($N_3D_3^+$) cannot be attributed to triazane alone.

3.3 Analysis of the middle *m/e* = 48 peak

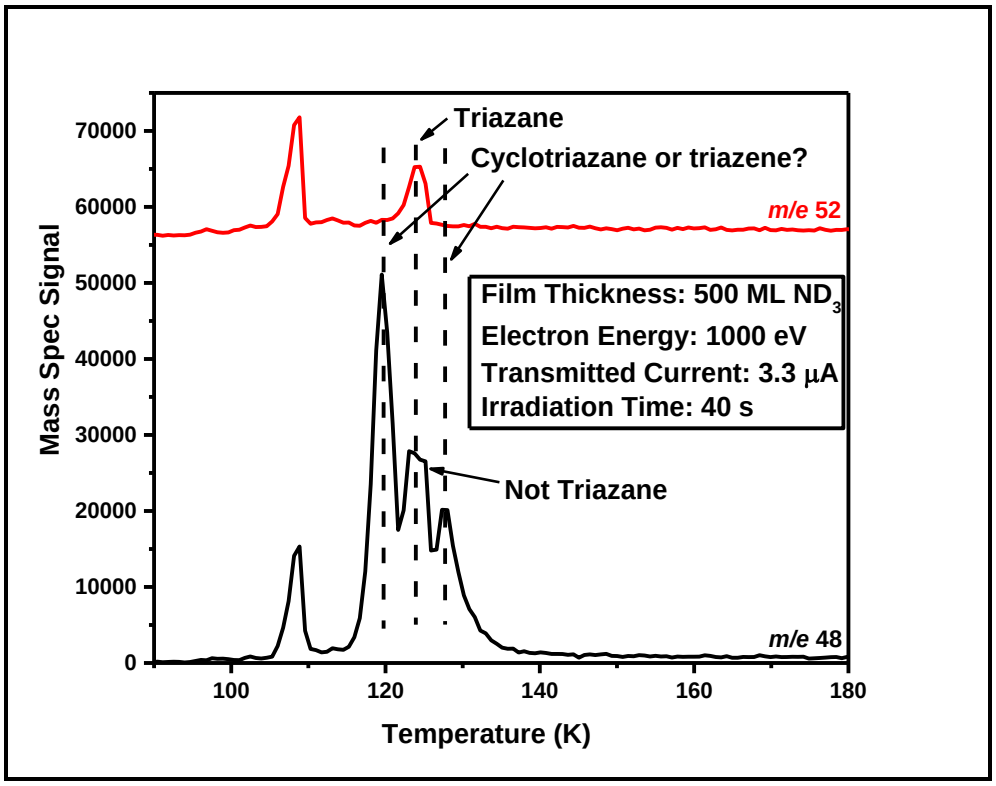

Figure 13

Post-irradiation temperature programmed desorption results of a 500 monolayer ND_3 film irradiated with 1000 eV electrons for 40 seconds at a dose rate of 3.3 μC/s.

Further post-irradiation temperature programmed desorption experiments were conducted in an attempt to identify the *m/e* = 48 peaks observed in Figure 12. When the incident electron current is increased, a third desorption feature is observed in the *m/e* = 48 signal (Figure 13). A comparison of the peaks in the *m/e* = 48 signal of these results to published data revealed several differences. In addition to the *m/e* = 48 peak that is aligned with the *m/e* = 52 peak, there are two other *m/e* = 48 peaks that we attribute to either cyclotriazane or triazene.

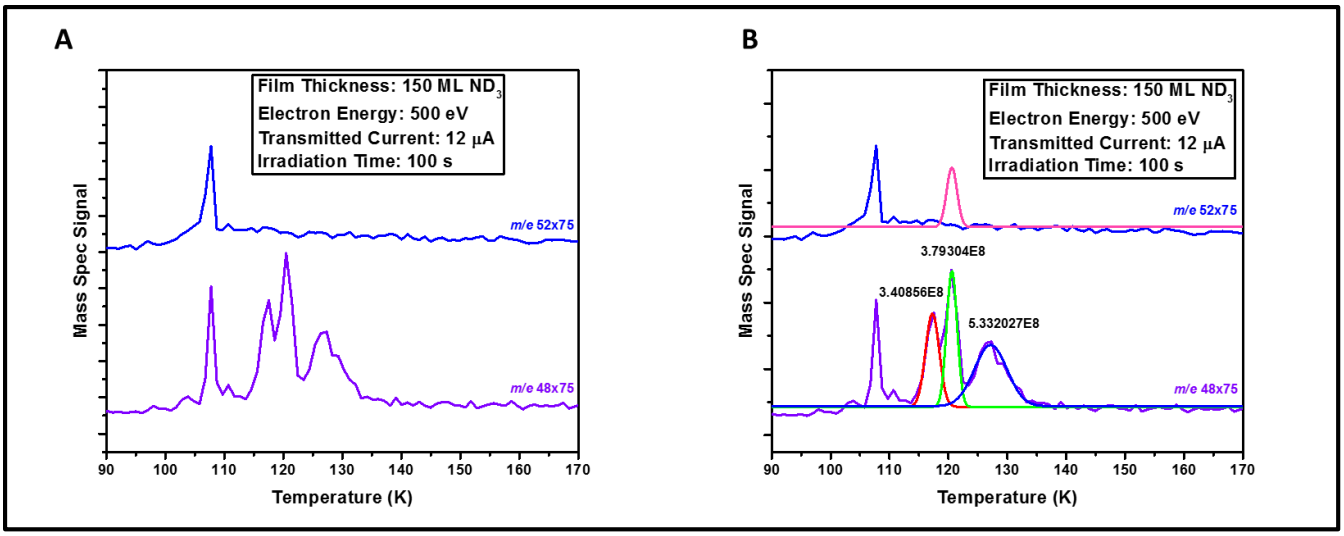

Figure 14

Post-irradiation temperature programmed desorption data following irradiation of 150 monolayer ND_3 film with 500 eV electrons. No triazane was observed (a). Calculations from previous experiments allowed us to determine what the *m/e* = 52 curve (pink) should be if the middle *m/e* = 48 peak was indeed a fragment of triazane. Gaussian curves used to determine the area under each of the three *m/e* = 48 peaks are shown in red, green, and blue (b).

When the energy of electrons used to irradiate the ammonia films was lowered to 500 eV, a peak in the *m/e* = 52 signal was no longer observed (Figure 14a). However, the *m/e* = 48 signal still consisted of three peaks. In order to investigate if the middle *m/e* = 48 peak could be due to a cracking fragment of triazane, data from a post-irradiation temperature programmed desorption experiment where both the *m/e* = 52 and *m/e* = 48 peaks were clearly present was analyzed (Figure 13). The amount of product corresponding to each peak was quantified by determining the area under the curve. The *m/e* = 52 peak area was calculated by simply integrating under the curve. Finding the area of the middle *m/e* = 48 peak proved to be more challenging as it required the three peaks to be deconvoluted. The area of the peak of interest was determined by fitting it to a Gaussian curve. The ratio of the middle *m/e* = 48 peak area to the *m/e* = 52 peak was found to be 2.3. If the middle *m/e* = 48 peak was indeed a cracking fragment of *m/e* = 52, then this ratio should remain the same across experiments so long as the mass spectrometer settings remain unchanged. Thus, the area of the middle *m/e* = 48 peak in Figure 14a was calculated and divided by 2.3 to obtain the

expected area of the *m/e* = 52 peak (Figure 14b). Because this ratio was not maintained across these experiments, we conclude that the middle *m/e* = 48 peak is not simply a cracking fragment of triazane, contrary to what was previously proposed [32].

3.4 Identification of *m/e* = 48 (N_3D_3)

While only one additional *m/e* = 48 peak was observed in the previous study, we observed two additional *m/e* = 48 peaks in our data [32]. Due to this difference in *m/e* = 48 peaks between our data and published data, 500 monolayer ND_3 films were irradiated for varying times (1-60 seconds) (Figure 15) to see if the *m/e* = 48 peaks would appear at different irradiation times. Different threshold irradiation times would suggest that the *m/e* = 48 peaks are not from the same molecular species.

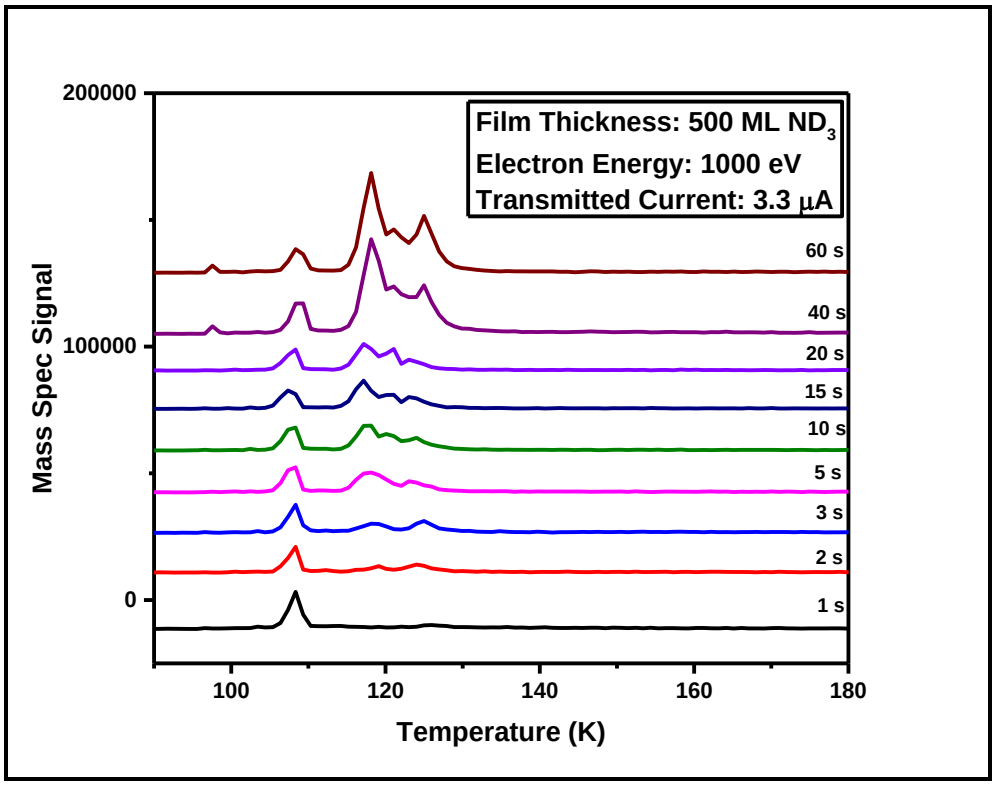

Figure 15

Post-irradiation temperature programmed desorption data after 500 ND_3 monolayer films were irradiated with 1000 eV electrons at an electron dose rate of 3.3 μC/s. Irradiation times were varied from 1 second to 60 seconds. The *m/e* = 48 product peaks appear together after a two second irradiation.

However, in all cases, the two *m/e* = 48 peaks that are misaligned with the *m/e* = 52 peak appeared together at the same irradiation time of two seconds, supporting our hypothesis that the two desorption peaks can be attributed to the same molecular species.

Additionally, the mass spectrometer electron energy was varied in an attempt to determine the identity of the N_3D_3 product (Figure 16).

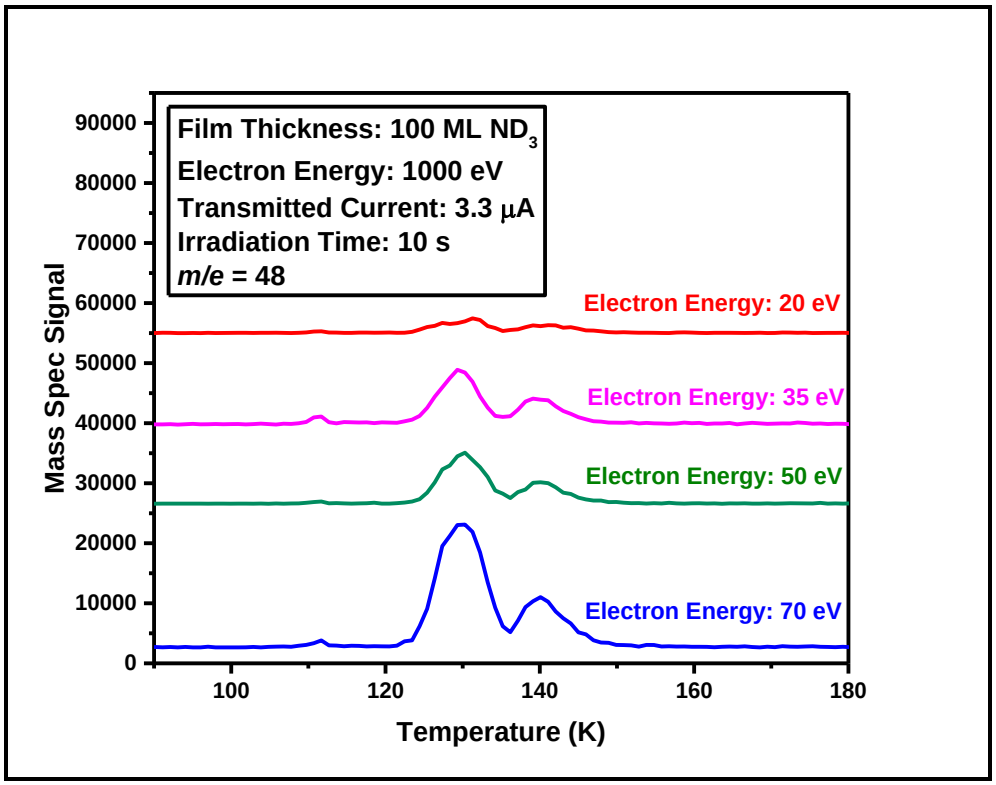

Figure 16

The *m/e* = 48 peaks disappear together as the mass spectrometer electron energy is lowered from 70 eV to 20 eV. The *m/e* = 48 signal was monitored following irradiation of a 100 monolayer ND_3 film for 10 seconds with 1000 eV electrons.

A mass spectrometer typically has its electron energy or ionization energy set at 70 eV. If two peaks were from two different molecular species, they would be expected to have different threshold ionization energies and would thus not disappear together as the electron energy is decreased. Upon lowering the electron energy to 20 eV, both of the *m/e* = 48 peaks began to diminish/disappear, suggesting that the desorption peaks are due to the same molecular species. We do concede, however, that the electron energy should have been reduced to an even lower energy, perhaps 15 eV, to provide conclusive evidence for our hypothesis. In contradiction to our claim, the relative ratios between the two desorption peaks appear to differ as the mass spectrometer electron energy is lowered. These experiments will have to be repeated in order to verify our conclusions.

3.5 Investigating the production of N-4 species

The formation of products with molar masses greater than 52 was also monitored during post-irradiation temperature programmed desorption experiments involving condensed ND_3. Following irradiation with 1000 eV electrons, a sharp peak was observed in *m/*e = 68 at 120 K. We initially attributed this peak to a new radiolysis product – tetrazane (N_4D_6).

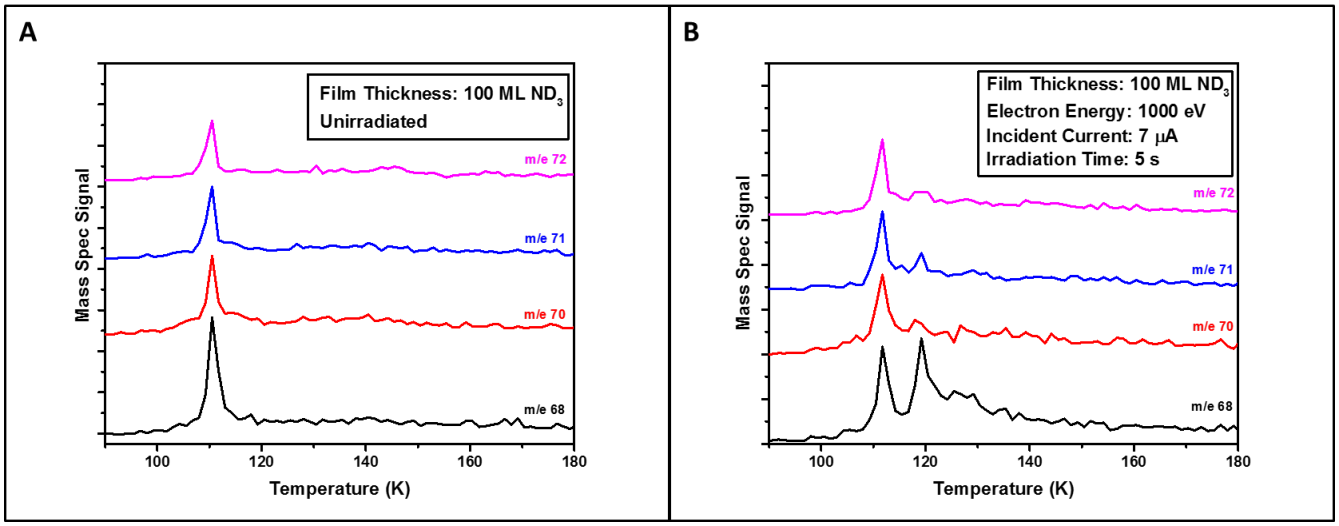

Figure 17

Post-irradiation temperature programmed desorption data for an unirradiated 100 monolayer ND_3 film (a) and a 100 monolayer ND_3 film irradiated with 1000 eV electrons for 5 seconds at an electron dose rate of 7 μC/s (b).

A control experiment (no irradiation) was done to ensure that this *m/*e = 68 peak was only observed after irradiating films of ammonia (Figure 17a). However, peaks in mass-to-charge ratios 70, 71, and 72 were also observed at the same desorption temperature following irradiation (Figure 17b). Because none of these mass-to-charge ratios correspond to tetrazane, our identification of tetrazane is inconclusive at best.

3.6 Hydrazine yield as a function of film thickness

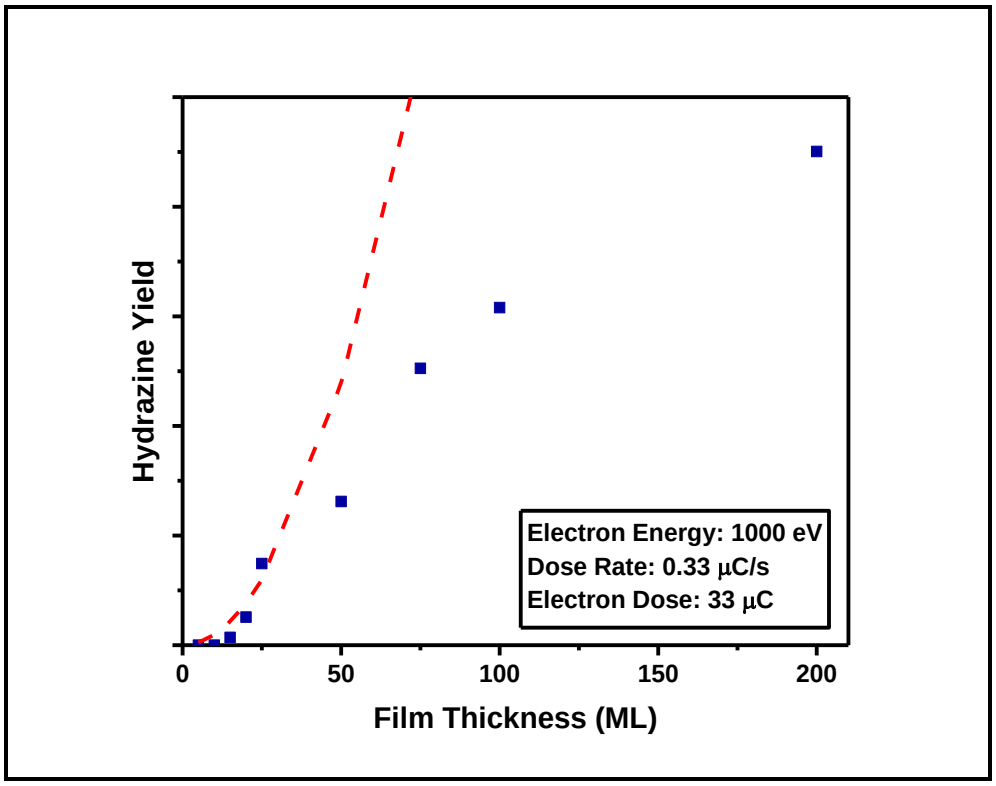

Figure 18

Hydrazine yield monitored as a function of film thickness. ND_3 films (5–200 monolayers) were irradiated with 1000 eV electrons at a dose rate of 0.33 μC/s for 100 seconds. The total electron dose was 33 μC. The data was then fit to a pure quadratic equation (red).

Films of ammonia ranging in thicknesses from 5 to 200 monolayers were grown on the Ta(110) crystal substrate and irradiated with 1000 eV electrons for a total electron dose of 33 μC (Figure 18). As the film thickness increased, the amount of hydrazine produced also increased. In order to quantify the yield of hydrazine, the *m/e* = 36 peak was integrated and the area under the curve was plotted against film thickness. The thinnest film in which hydrazine was detected was 15 monolayers. Because the first five data points fit well with a pure quadratic equation (r = 0.82829), this data is suggestive of a bimolecular reaction mechanism for the production of hydrazine. As the film thickness is increased beyond 25 monolayers, the yield begins to plateau, likely due to the finite mean free path of a 1000 eV electron (~10 Å) [41].

3.7 Diazene yield as a function of film thickness

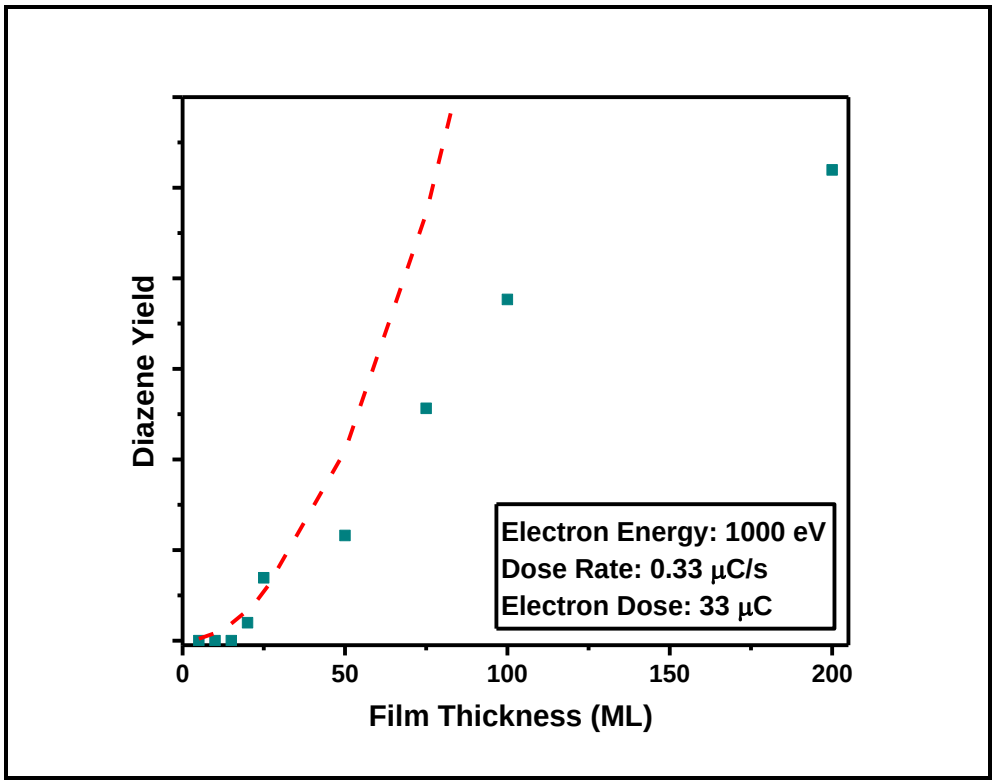

Figure 19

Diazene yield monitored as a function of film thickness. ND_3 films (5–200 monolayers) were irradiated with 1000 eV electrons at a dose rate of 0.33 μC/s for 100 seconds. The total electron dose was 33 μC. The data was then fit to a pure quadratic equation (red).

In the same set of experiments described in the previous section, the yield of diazene was monitored as a function of film thickness (Figure 19). Similar results were observed; the yield of diazene increased as the ND_3 film thickness was increased.

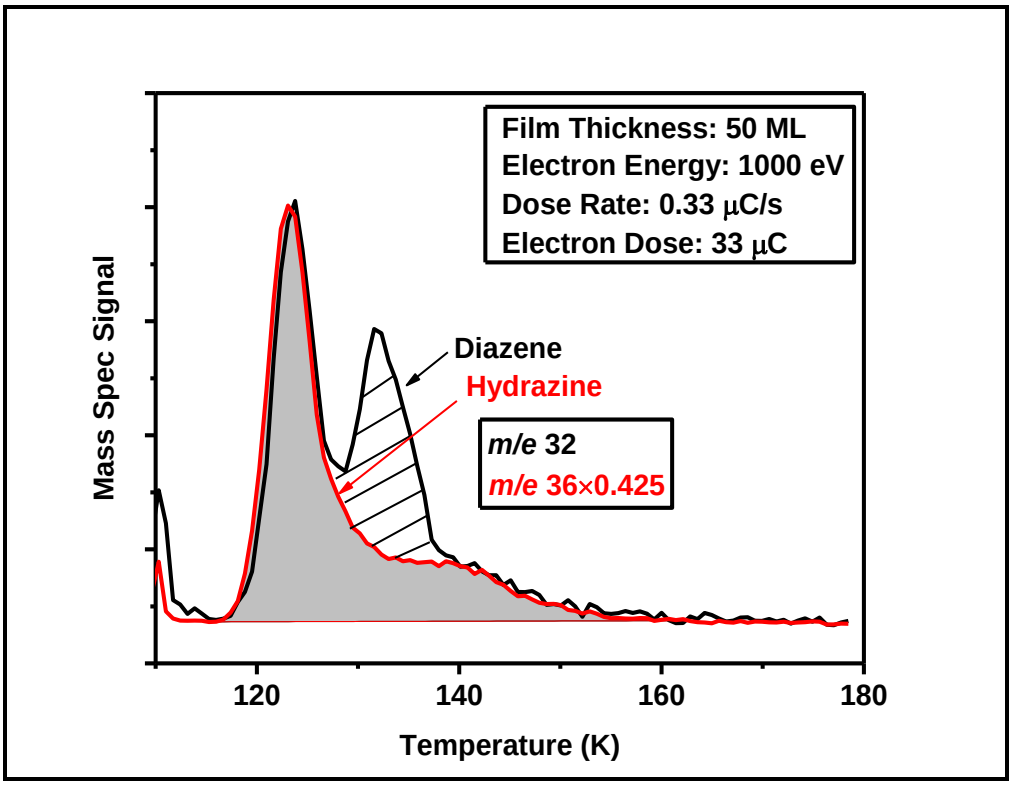

Figure 20

Calculating diazene yield from post-irradiation temperature programmed desorption data. The *m/e* = 36 mass spectra curve is multiplied by some factor in order to overlay its hydrazine peak at 124 K with its fragment peak in *m/e* = 32. The area under the *m/e* = 36 curve is subtracted from the area under the *m/e* = 32 curve. The striped region shown corresponds to diazene product.

The quantification of diazene required additional calculations to ensure that the integration of the relevant *m/e* = 32 curve did not include any contribution from hydrazine (Figure 20). This separation was accomplished by first multiplying the *m/e* = 36 curve by a factor such that this hydrazine curve would overlay on the *m/e* = 32 curve corresponding to both hydrazine and diazene. Finally, the area under the modified *m/e* = 36 curve was subtracted from the area under the *m/e* = 32 curve in order to quantify the amount of *m/e* = 32 that was exclusive to the diazene product.

3.8 Hydrazine yield as a function of fluence

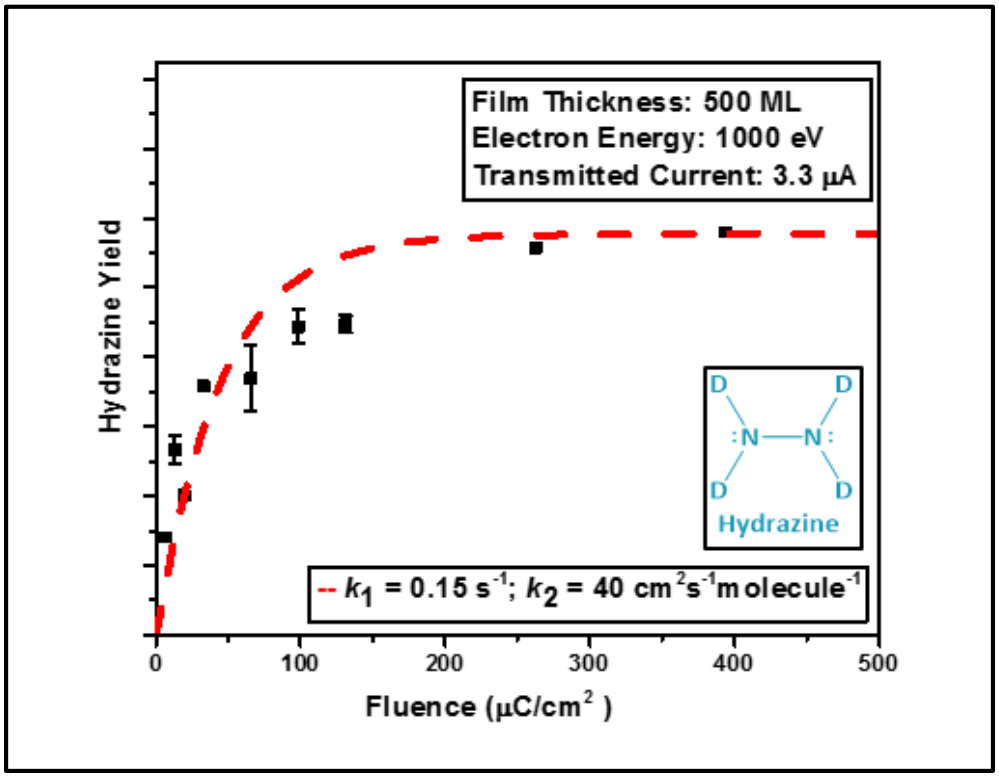

Figure 21

Hydrazine yield as a function of fluence. ND_3 films (500 monolayers) were irradiated with 1000 eV electrons. Irradiation times were varied from 1 second to 60 seconds while the current transmitted on the crystal was maintained at 3.3 μA.

The yield of hydrazine was monitored as a function of fluence (Figure 21) at constant film thickness. This was accomplished by maintaining the same flux across experiments and varying the irradiation times. The data was fitted using a model for hydrazine production described in a previous Wellesley College thesis [42]. For the formation of hydrazine product, this model proposes a bimolecular mechanism, which begins with the generation of NH_2 radicals resulting from the bombardment of ammonia films with electrons. Following the first step of this reaction, two NH_2 radicals can then combine to produce a hydrazine molecule. Differential equations can be written for each step of this proposed mechanism, where the R is NH_3, the I is the NH_2 radical intermediate, and the P is hydrazine.

$$\frac{\mathrm{d[R]}}{\mathrm{d}t} = -k_1[\mathrm{R}] \tag{5}$$

$$\frac{\mathrm{d[I]}}{\mathrm{d}t} = k_1[\mathrm{R}] - k_2[\mathrm{I}]^2 \tag{6}$$

$$\frac{\mathrm{d[P]}}{\mathrm{d}t} = k_2[\mathrm{I}]^2 \tag{7}$$

3.9 Diazene yield as a function of fluence

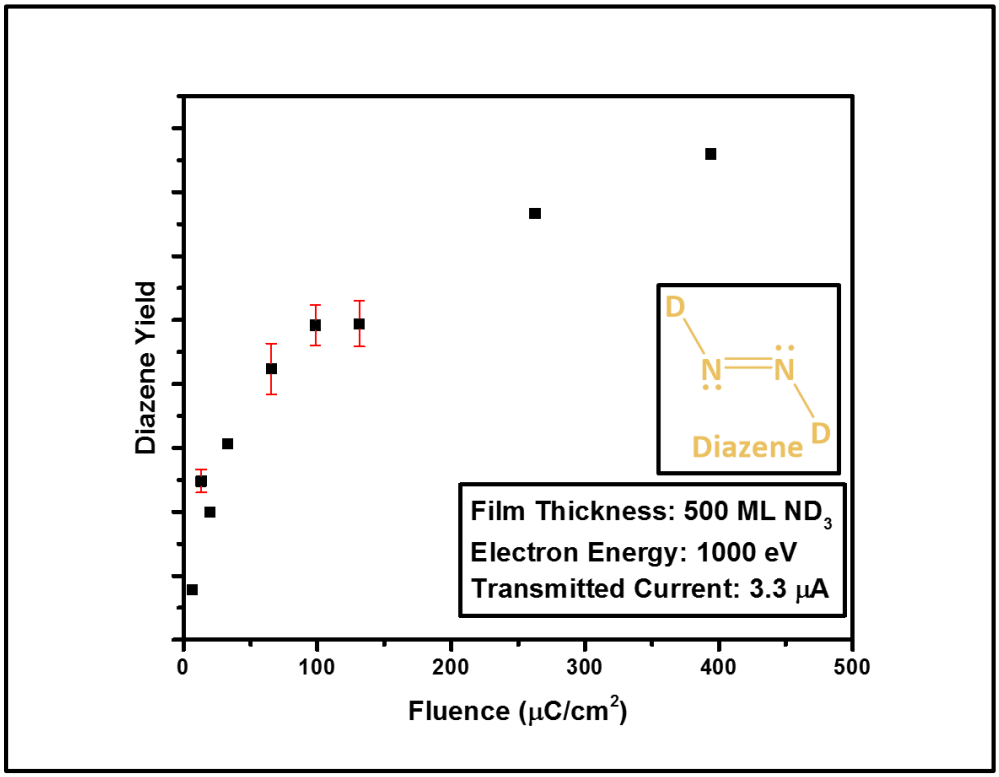

Figure 22

Diazene yield as a function of fluence. ND_3 films (500 monolayers) were irradiated with 1000 eV electrons. Irradiation times were varied from 1 second to 60 seconds while the current incident on the crystal was maintained at 3.3 μA.

As mentioned previously, prior studies have proposed two possible mechanisms for diazene production – (1) two NH radicals combining to make diazene and (2) an excited-state hydrazine molecule dissociating into diazene and H_2 [30] (Figure 4). The diazene yield was thus monitored as a function of irradiation time in order to determine the more likely mechanism for electron-induced diazene formation (Figure 22). The results were suggestive of a mechanism

similar to that of hydrazine formation. As such, it is proposed that the mechanism for the formation of diazene involves two NH radicals joining together.

3.10 Detection of N-2 species at low-electron energies (30 eV)

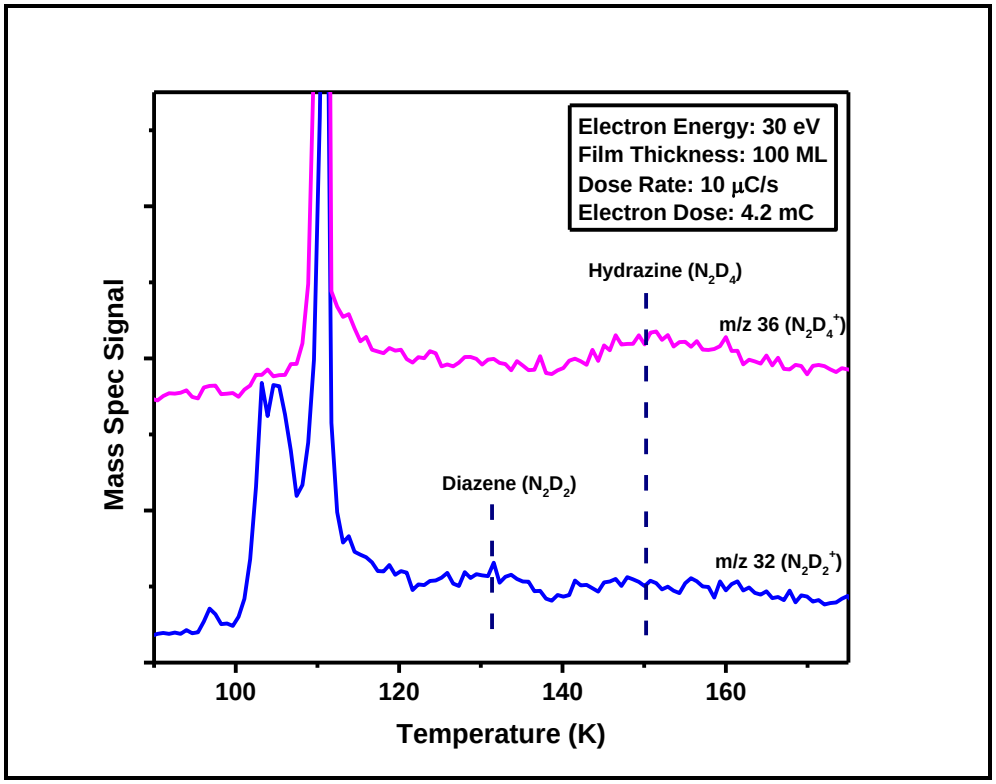

Figure 23

Post-irradiation temperature programmed desorption data following the irradiation of a 100 monolayer ND_3 film with 30 eV electrons for 7 minutes at a dose rate of 10 μC/s. Desorption temperatures of hydrazine and diazene switch.

Because our laboratory's ultimate goal is to investigate the role of low-energy electrons in the radiolysis of ammonia, we conducted temperature programmed desorption experiments at lower incident electron energies. The lowest incident electron energy at which hydrazine and diazene production were consistently observed was 30 eV (Figure 23). Calculations of product yields reveal that the amount of hydrazine and diazene produced is considerably smaller than those of analogous post-irradiation temperature programmed desorption experiments conducted with 1000 eV electrons. It is interesting to note that at 30 eV, the desorption temperatures of the products

switch. When there are small amounts of diazene and hydrazine being formed, diazene desorbs before hydrazine, as is expected for a lower mass reaction product.

3.11 Triazane yield as a function of fluence

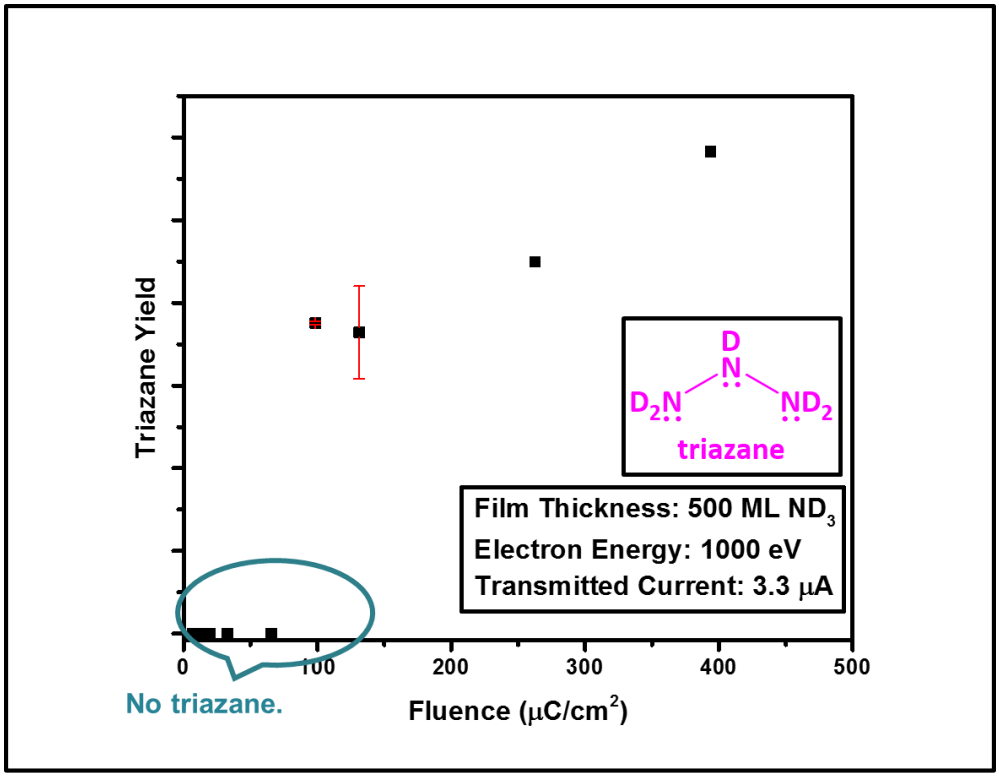

Figure 24

Triazane yield as a function of fluence. ND_3 films (500 monolayers) were irradiated with 1000 eV electrons. Irradiation times were varied from 1 second to 60 seconds while the current incident on the crystal was maintained at 3.3 μA.

Similarly, the production of the N-3 species – triazane (N_3D_5) and cyclotriazane/triazene (N_3D_3) – was also investigated as a function of incident electron fluence. Triazane production was only observed following irradiation for at least 15 seconds (Figure 24). This finding suggests that triazane is a tertiary product of electron-induced ammonia radiolysis. As a result, a mechanism for the formation of triazane that involves a series of steps can be proposed (Figure 25). First, two NH_2 radicals combine together to form hydrazine. Upon interaction with another electron, this hydrazine molecule can be excited and can subsequently dissociate into a hydrazinyl (N_2H_3)

radical intermediate and a hydrogen radical. Lastly, an additional NH_2 radical can be inserted into the N_2H_3 radical to yield triazane. Previous studies have observed the formation of triazane after exposing hydrazine to an electrodeless discharge lamp [43]. These results are consistent with our proposed mechanism for triazane production.

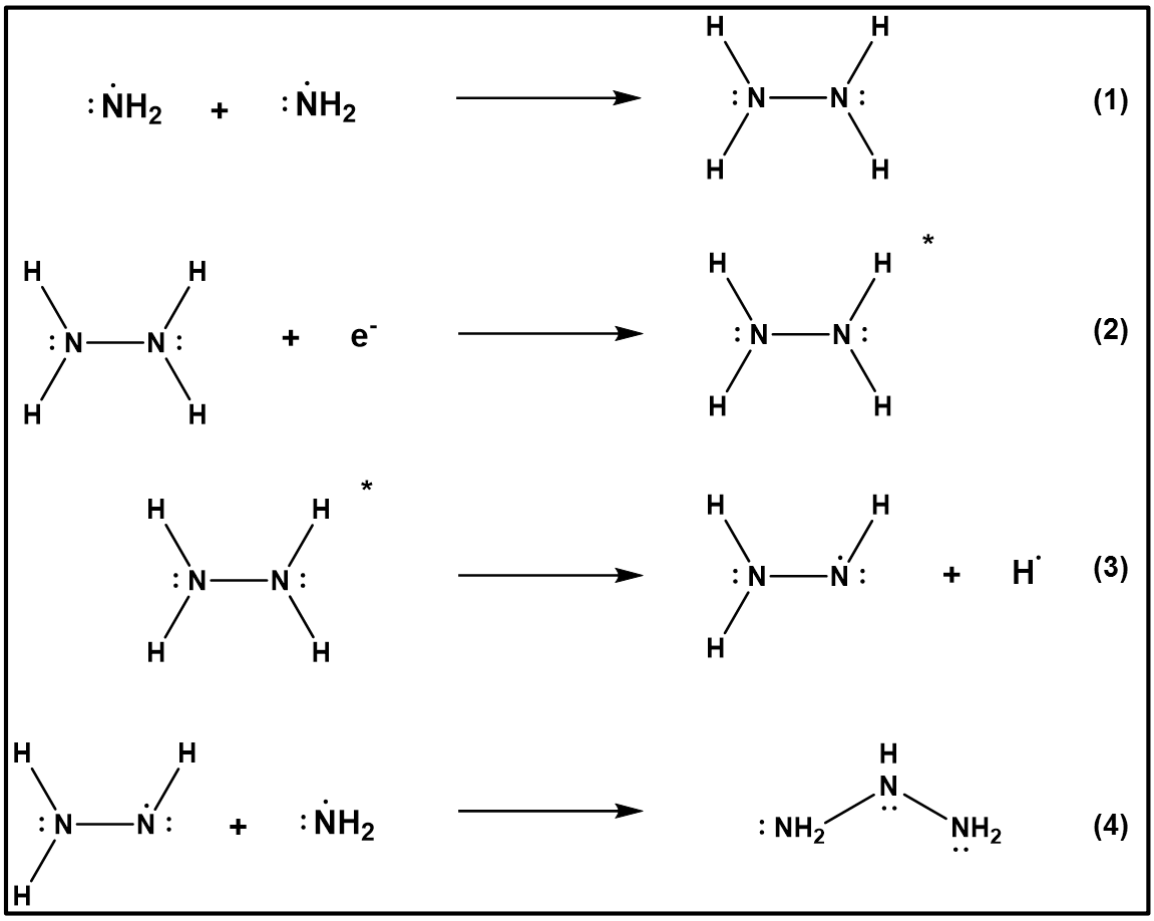

Figure 25
Proposed mechanism for triazane (N_3H_5) formation.

3.12 N_3D_3 yield as a function of fluence

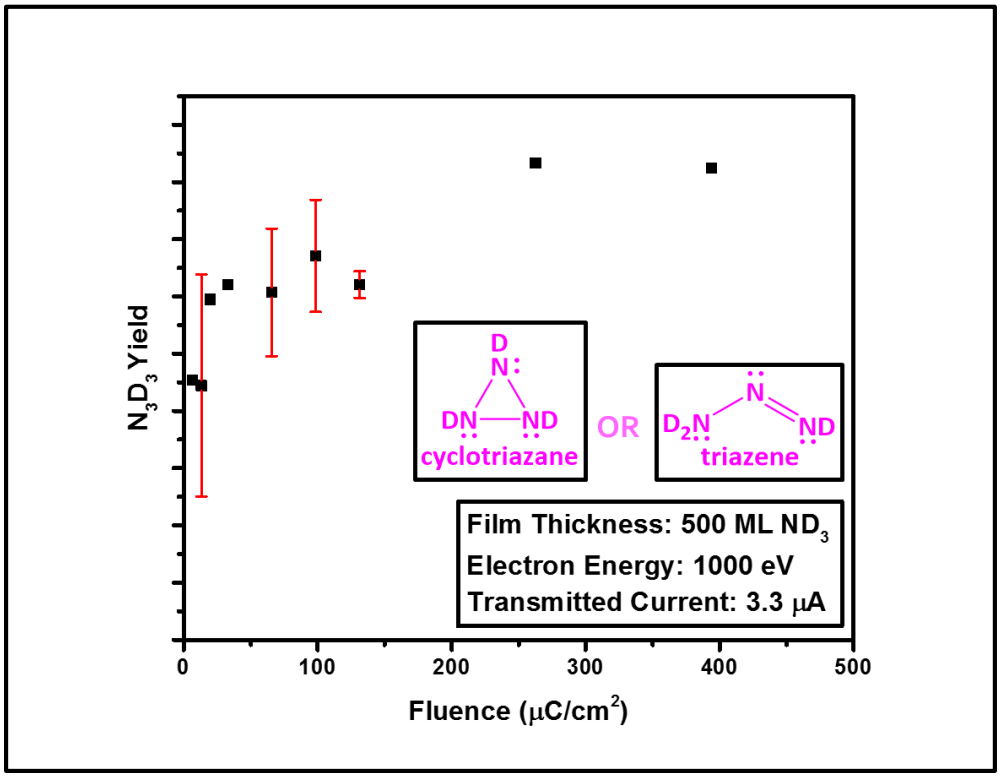

Figure 26

N_3D_3 yield as a function of fluence. 500 monolayer ND_3 films were irradiated with 1000 eV electrons. Irradiation times were varied from 1 second to 60 seconds while the current incident on the crystal was maintained at 3.3 μC.

In contrast, yield versus irradiation time data for N_3D_3 indicates the production of this N-3 species even at low irradiation times (Figure 26). This finding suggests a one-step mechanism, in which 3 ND radicals combine together to form cyclotriazane, which is likely a secondary radiolysis product.

3.13 Dose Rate Effect

3.13.1 No triazane following irradiation with 500 eV electrons.

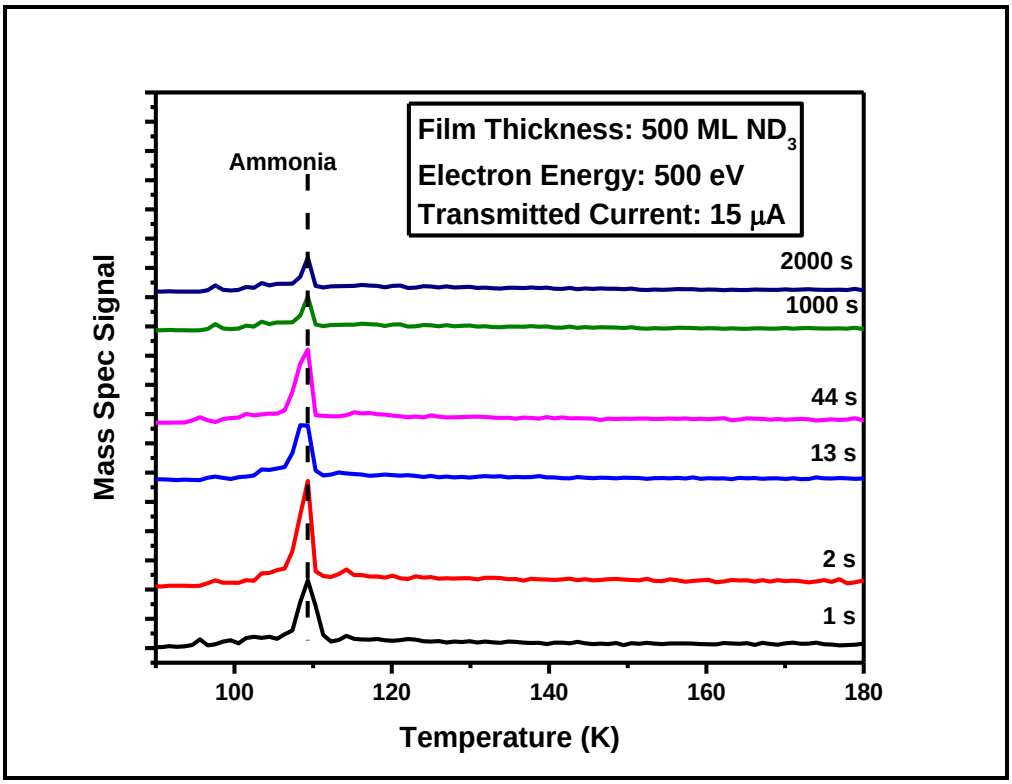

Figure 27

500 monolayer ND_3 films were irradiated with 500 eV electrons at a dose rate of 15 μC/s for 1 second to 2000 seconds. No triazane production was observed.

Given the appropriate experimental parameters (500 monolayer ND_3, 3.3 μA), the production of triazane is consistently observed after irradiating ammonia films with 1000 eV electrons. However, when an identical ammonia film is irradiated with 500 eV electrons, the production of triazane is no longer observed (Figure 27). Further experiments with irradiation times ranging from 5 s to 2000 s were conducted, and triazane production was still not observed. Many other experimental parameters were varied at an incident electron energy of 500 eV; however, the production of triazane at 500 eV was not observed (Table 1).

Electron Energy (eV)	Film Thickness (ML)	Irradiation Time (s)	Transmitted Current (μA)
500	500	5	3.3
500	500	10	3.3
500	500	15	3.3
500	500	20	3.3
500	500	30	3.3
500	500	40	3.3
500	500	60	3.3
500	500	100	3.3
500	500	200	3.3
500	500	1	15
500	500	2	15
500	500	13	15
500	500	44	15
500	500	2000	15
500	500	40	15
500	150	40	8
500	150	80	8
500	150	100	8
500	150	100	12
500	150	80	12
500	150	60	12
500	150	120	8
500	150	300	8
500	150	40	15
500	100	40	8
500	100	300	8
500	75	40	8
500	50	40	10

Table 1

Experiments conducted at an electron energy of 500 eV. No triazane was observed during any of these experiments.

There is no known electron-induced phenomenon that turns on above 500 eV, though a dose rate effect may provide an explanation for this interesting observation. Irradiation with 500 eV electrons likely produces a lower density of secondary electrons and radicals than irradiation with 1000 eV electrons. Therefore, at 500 eV, we propose that radicals are not produced sufficiently close together to interact and combine to form product before they diffuse away from each other.

As a result, observation of triazane production with 500 eV electrons may require incident currents that cannot be experimentally achieved with our electron gun. We plan to conduct experiments involving the irradiation of 500 monolayer films with electron energies intermediate to 500 eV and 1000 eV in order to further investigate this phenomenon and determine an apparent electron energy threshold for the production of triazane.

3.13.2 Dose rate effect for N-2 radiolysis products

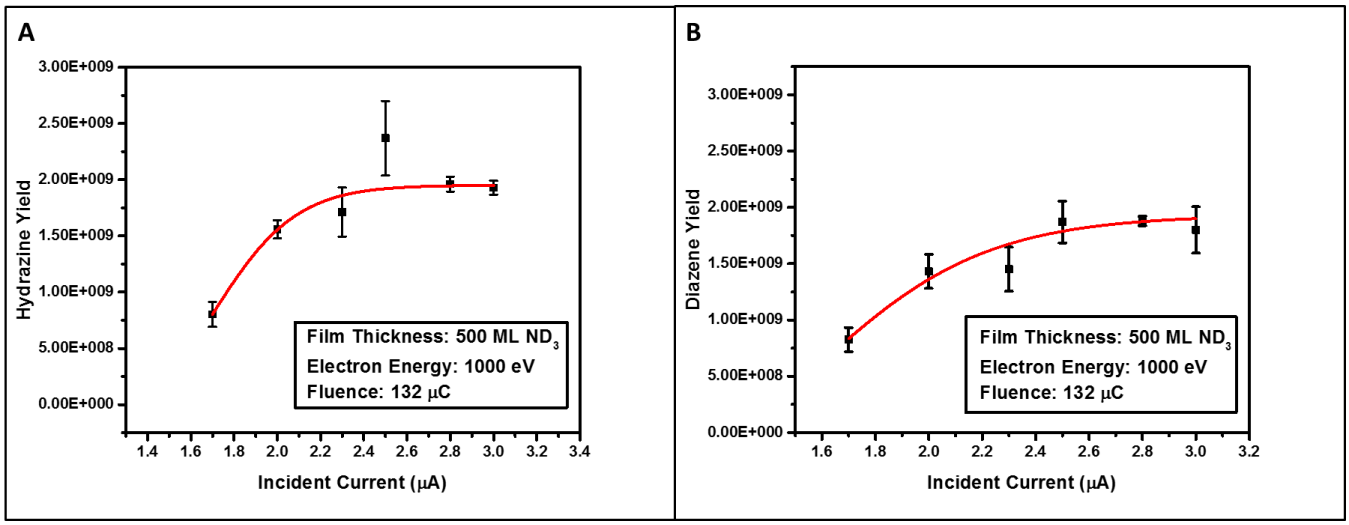

Figure 28

ND_3 (500 monolayer) films were irradiated with 1000 eV electrons for a total electron dose of 132 μC. Flux and irradiation times were varied during these experiments. The yields of hydrazine (a) and the yields of diazene (b) are plotted as a function of incident current. Data was fit to a logarithmic function for visual guidance (red).

The dose rate effect for the electron-induced production of ammonia radiolysis products was investigated by conducting experiments that maintained a constant fluence. The current incident on the crystal and irradiation time were then varied accordingly. Results of these experiments show a clear dose rate effect for the production of both hydrazine and diazene (Figure 28). The red curve is simply used to guide the reader's eye and has no mathematical basis. As the incident current was increased, the yield of the two N-2 radiolysis products also increased. This result violates the Bunsen-Roscoe Law of Photochemistry, which would predict that the yield of

these two products would remain the same as the electron dose was kept constant across experiments.

3.13.3 Dose rate effect for N-3 radiolysis products

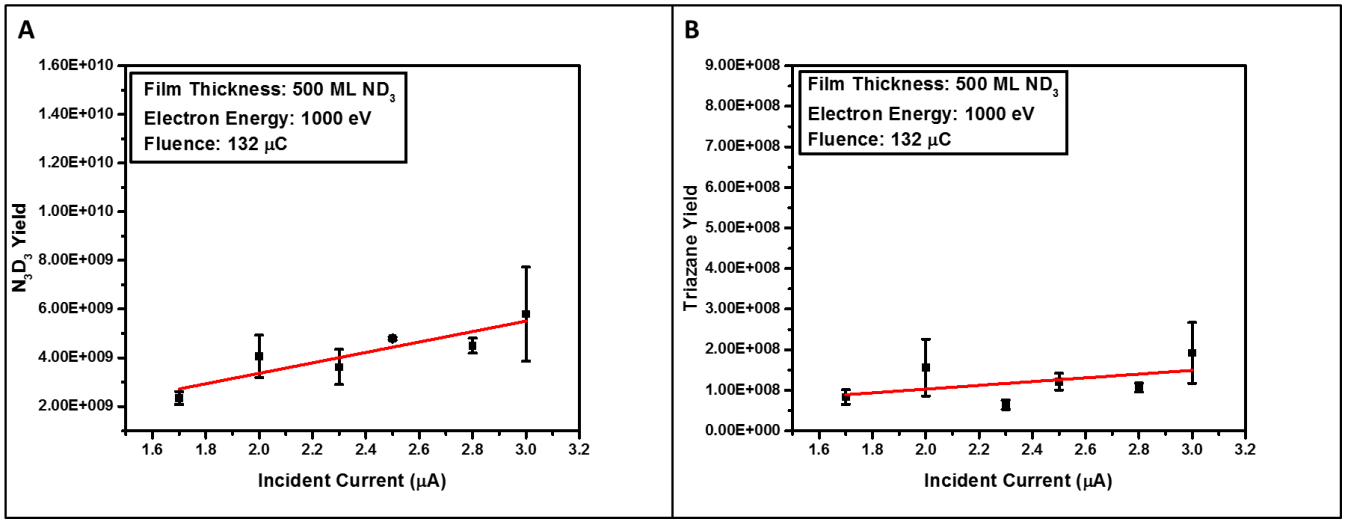

Figure 29

ND_3 (500 monolayers) films were irradiated with 1000 eV electrons for a total electron dose of 132 μC. Flux and irradiation times were varied during these experiments. The yields of N_3D_3 (a) and the yields of triazane (b) are plotted as a function of incident current. Data was fit to a linear function for visual guidance (red).

Data from dose rate effect experiments for N_3D_3 and triazane was fit linearly (Figure 29). The linear functions shown in red have no mathematical basis and are simply used to guide the reader's eye. While the evidence for the dose rate effect for N_3D_3 and triazane is not as conclusive, it is predicted that a different range of incident currents would demonstrate a stronger dose rate effect.

4 Conclusion

Post-irradiation temperature programmed desorption experiments conducted in our laboratory have successfully observed the electron-induced production of hydrazine (N_2H_4), diazene (N_2H_2), cyclotriazane/triazene (N_3H_3), and triazane (N_3H_5) from condensed ammonia. Further experiments

were performed to investigate the yield of these N-2 and N-3 radiolysis products as a function of irradiation time, film thickness, electron energy, and incident current. From yield versus irradiation time and yield versus film thickness results, we suggest that both hydrazine and diazene are formed via a bimolecular reaction mechanism. Analogous yield versus irradiation results for triazane allowed us to conjecture that triazane is a tertiary radiolysis product of ammonia. The N_3H_3 species detected following irradiation of ammonia films with electrons is likely cyclotriazane**,** as it is produced at very low irradiation times. Lastly, we attribute the nondetection of triazane at 500 eV to a dose rate effect. We believe that the detection of triazane at this electron energy would require incident currents that are unachievable with an electron gun. Furthermore, a clear dose rate effect has been observed with hydrazine and diazene. A similar result is expected with the N-3 species at a different incident current range. We speculate that triazane would be produced at lower incident electron energies in cosmic ices bombarded by intense high energy cosmic rays (Figure 30).

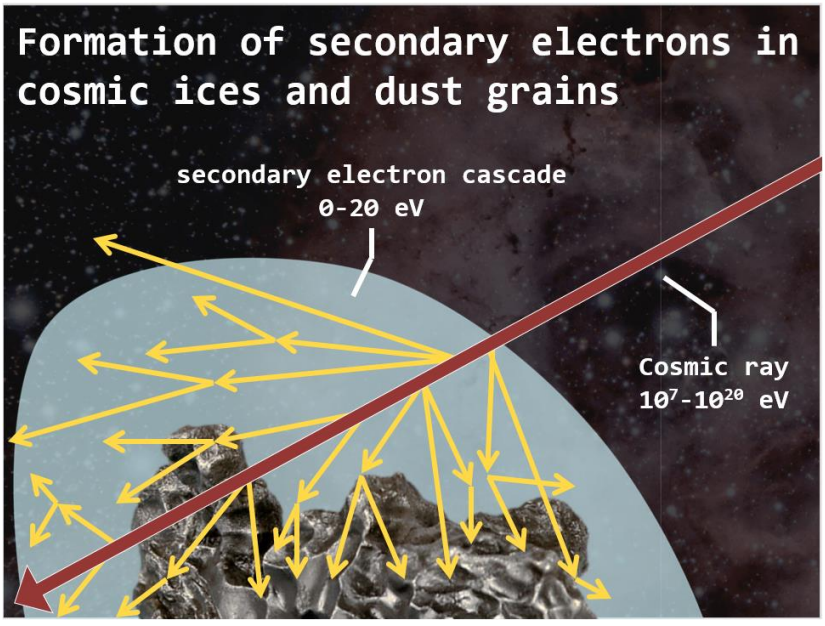

Figure 30
Cosmic ices in the interstellar medium are bombarded with high-energy radiation such as cosmic rays (10^7-10^{20} eV) to yield a cascade of secondary electrons (0-20 eV).

5 References

[1] L.D. Weeks, L.L. Zhu, M. Pellon, D.R. Haines, C.R. Arumainayagam, Low-energy electron-induced oligomerization of condensed carbon tetrachloride, The Journal of Physical Chemistry C 111 (2007) 4815-4822.

[2] G.M. Munoz Caro, E. Dartois, Prebiotic chemistry in icy grain mantles in space. An experimental and observational approach, Chemical Society reviews 42 (2013) 2173-2185.

[3] J.P. Bernard, D. Paradis, D.J. Marshall, L. Montier, G. Lagache, R. Paladini, M. Veneziani, C.M. Brunt, J.C. Mottram, P. Martin, I. Ristorcelli, A. Noriega-Crespo, M. Compiegne, N. Flagey, L.D. Anderson, C.C. Popescu, R. Tuffs, W. Reach, G. White, M. Benedetti, L. Calzoletti, A.M. DiGiorgio, F. Faustini, M. Juvela, C. Joblin, G. Joncas, M.A. Mivilles-Deschenes, L. Olmi, A. Traficante, F. Piacentini, A. Zavagno, S. Molinari, Dust temperature tracing the ISRF intensity in the Galaxy, Astron. Astrophys. 518 (2010).

[4] J.G. Mangum, A. Wootten, Formaldehyde as a Probe of Physical Conditions in Dense Molecular Clouds, Astrophys J Suppl S 89 (1993) 123-153.

[5] P. Ehrenfreund, S.B. Charnley, Organic molecules in the interstellar medium, comets, and meteorites: A voyage from dark clouds to the early earth, Annu Rev Astron Astr 38 (2000) 427-+.

[6] P. de Marcellus, C. Meinert, I. Myrgorodska, L. Nahon, T. Buhse, L.L. d'Hendecourt, U.J. Meierhenrich, Aldehydes and sugars from evolved precometary ice analogs: Importance of ices in astrochemical and prebiotic evolution, Proc. Natl. Acad. Sci. U. S. A. 112 (2015) 965-970.

[7] R.T. Garrod, S.L.W. Weaver, Simulations of Hot-Core Chemistry, Chem. Rev. 113 (2013)

8939-8960.

[8] C.J. Shen, J.M. Greenberg, W.A. Schutte, E.F. van Dishoeck, Cosmic ray induced explosive chemical desorption in dense clouds, Astron. Astrophys. 415 (2004) 203-215.

[9] D.E. Woon, Pathways to glycine and other amino acids in ultraviolet-irradiated astrophysical ices determined via quantum chemical modeling, Astrophysical Journal 571 (2002) L177-L180.

[10] P. de Marcellus, M. Bertrand, M. Nuevo, F. Westall, L.L. d'Hendecourt, Prebiotic Significance of Extraterrestrial Ice Photochemistry: Detection of Hydantoin in Organic Residues, Astrobiology 11 (2011) 847-854.

[11] F. Borget, G. Danger, F. Duvernay, M. Chomat, V. Vinogradoff, P. Theule, T. Chiavassa, Aminoacetonitrile characterization in astrophysical-like conditions, Astron. Astrophys. 541 (2012).

[12] S.K. Atreya, P.R. Mahaffy, H.B. Niemann, M.H. Wong, T.C. Owen, Composition and origin of the atmosphere of Jupiter - an update, and implications for the extrasolar giant planets, Planet Space Sci. 51 (2003) 105-112.

[13] M.D. Hofstadter, D.O. Muhleman, Latitudinal Variations of Ammonia in the Atmosphere of Uranus - an Analysis of Microwave Observations, Icarus 81 (1989) 396-412.

[14] G.F. Lindal, The Atmosphere of Neptune - an Analysis of Radio Occulation Data Acquired with Voyager-2, Astron. J. 103 (1992) 967-982.

[15] J.M. Bauer, T.L. Roush, T.R. Geballe, K.J. Meech, T.C. Owen, W.D. Vacca, J.T. Rayner, K.T.C. Jim, The near infrared spectrum of Miranda - Evidence of crystalline water ice, Icarus 158 (2002) 178-190.

[16] S. Wyckoff, S.C. Tegler, L. Engel, Ammonia Abundances in 4 Comets, Astrophysical

Journal 368 (1991) 279-286.

[17] J.M. Greenberg, C. Vandebult, L.J. Allamandola, Ices in Space, J. Phys. Chem. 87 (1983) 4243-4260.

[18] K.I. Oberg, A.C.A. Boogert, K.M. Pontoppidan, S. van den Broek, E.F. van Dishoeck, S. Bottinelli, G.A. Blake, N.J. Evans, THE SPITZER ICE LEGACY: ICE EVOLUTION FROM CORES TO PROTOSTARS, Astrophysical Journal 740 (2011).

[19] T.L. Roush, Physical state of ices in the outer solar system, J. Geophys. Res.-Planets 106 (2001) 33315-33323.

[20] D.P. Zaleski, N.A. Seifert, A.L. Steber, M.T. Muckle, R.A. Loomis, J.F. Corby, O. Martinez, K.N. Crabtree, P.R. Jewell, J.M. Hollis, F.J. Lovas, D. Vasquez, J. Nyiramahirwe, N. Sciortino, K. Johnson, M.C. McCarthy, A.J. Remijan, B.H. Pate, Detection of E-Cyanomethanimine toward Sagittarius B2(N) in the Green Bank Telescope Primos Survey, Astrophys J Lett 765 (2013).

[21] C. Lefevre, L. Pagani, M. Juvela, R. Paladini, R. Lallement, D.J. Marshall, M. Andersen, A. Bacmann, P.M. McGehee, L. Montier, A. Noriega-Crespo, V.M. Pelkonen, I. Ristorcelli, J. Steinacker, Dust properties inside molecular clouds from coreshine modeling and observations, Astron. Astrophys. 572 (2014).

[22] C.R. Arumainayagam, H.-L. Lee, R.B. Nelson, D.R. Haines, R.P. Gunawardane, Low-energy electron-induced reactions in condensed matter, Surface Science Reports 65 (2010) 1-44.

[23] C.R. Arumainayagam, Lee,H. D., Nelson, R. B., Haines, D.R., Gunawardane, R., Low-Energy Electron-Induced Reactions in Condensed Matter, Surface Science Reports 65 (2010) 1–44.

[24] M.D. Boamah, Sullivan, K. K., Shulenberger, K. E., Soe, C. M., Jacobs, L. M., Yhee, F. C., Atkinson, K. E., Boyer, M. C., Haines, D. R., Arumainayagam, C. R., Low-Energy Electron-Induced Chemistry of Condensed Methanol: Implications for the Interstellar Synthesis of Prebiotic Molecules, Faraday Discussions 168 (2014).

[25] X.L. Zhou, J.M. White, PHOTON-INDUCED AND ELECTRON-INDUCED CHEMISTRY OF CHLOROBENZENE ON AG(111), Journal of Chemical Physics 92 (1990) 5612-5621.

[26] S.C. Sparks, A. Szabo, G.J. Szulczewski, K. Junker, J.M. White, Thermal, electron, and photon induced chemistry of acetone on Ag(111), Journal of Physical Chemistry B 101 (1997) 8315-8323.

[27] R.L. Hudson, M.H. Moore, The N-3 radical as a discriminator between ion-irradiated and UV-photolyzed astronomical ices, Astrophysical Journal 568 (2002) 1095-1099.

[28] Y.J. Chen, A. Ciaravella, G.M.M. Caro, C. Cecchi-Pestellini, A. Jimenez-Escobar, K.J. Juang, T.S. Yih, SOFT X-RAY IRRADIATION OF METHANOL ICE: FORMATION OF PRODUCTS AS A FUNCTION OF PHOTON ENERGY, Astrophysical Journal 778 (2013) 162 161-111.

[29] A. Ciaravella, G.M. Caro, A.J. Escobar, C. Cecchi-Pestellini, S. Giarrusso, M. Barbera, A. Collura, Soft X-Ray Irradiation of Methanol Ice: Implication for H2co Formation in Interstellar Regions, Astrophys J Lett 722 (2010) L45-L48.

[30] W.J. Zheng, D. Jewitt, Y. Osamura, R.I. Kaiser, Formation of nitrogen and hydrogen-bearing molecules in solid ammonia and implications for solar system and interstellar ices, Astrophysical Journal 674 (2008) 1242-1250.

[31] K. Shulenberger, Radiolysis of Astrochemically Relevant Ammonia Ices by Low- and High-Energy Electrons, Chemistry, Wellesley College, Wellesley, MA, 2014.

[32] M. Förstel, P. Maksyutenko, B.M. Jones, B.J. Sun, S.H. Chen, A. Chang, R.I. Kaiser, Detection of the Elusive Triazane Molecule (N3H5) in the Gas Phase, ChemPhysChem 16 (2015) 3139-3142.

[33] M. Guilhaus, Principles and Instrumentation in Time-of-Flight Mass Spectrometry, JOURNAL OF MASS SPECTROMETRY 30 (1995) 1532.

[34] B. Mamyrin, V. Karataev, D. Shmikk, V. Zagulin, The mass-reflectron, a new nonmagnetic time-of-flight mass spectrometer with high resolution, Zh. Eksp. Teor. Fiz 64 (1973) 82-89.

[35] H.B. Schlegel, A. Skancke, Thermochemistry, Energy Comparisons, and Conformational-Analysis of Hydrazine, Triazane, and Triaminoammonia, Journal of the American Chemical Society 115 (1993) 7465-7471.

[36] D.H. Magers, E.A. Salter, R.J. Bartlett, C. Salter, B.A. Hess, L. Schaad, Do stable isomers of N3H3 exist?, Journal of the American Chemical Society 110 (1988) 3435-3446.

[37] E.J. Hall, Radiation dose-rate: a factor of importance in radiobiology and radiotherapy, The British journal of radiology 45 (1972) 81-97.

[38] A. Mozumder, J. Magee, Theory of radiation chemistry. VII. Structure and reactions in low LET tracks, The Journal of Chemical Physics 45 (1966) 3332-3341.

[39] H.L. Tavernier, Efficient Design of a Chamber for Ultrahigh Vacuuma nd Elevated Pressure Surface Studies, Chemistry, Wellesley College, Wellesley, 1994.

[40] P. Hawkes, Spence, J., Science of Microscopy, 2007.

[41] J. Ashley, Interaction of low-energy electrons with condensed matter: stopping powers and inelastic mean free paths from optical data, Journal of electron spectroscopy and related phenomena 46 (1988) 199-214.

[42] K. Tran, Quantitative Investigations of Ammonia, Chemistry, Wellesley College, Wellesley, M.A., 2015.

[43] S. Foner, R.L. Hudson, Mass Spectrometric Detection of Triazene and Tetrazene and Studies of the Free Radicals NH2 and N2H3, The Journal of Chemical Physics 29 (1958) 442-443.